# STEADY-STATE ANALYSIS OF DEW-POINT EVAPORATIVE COOLING SYSTEM

楊, 程
九州大学大学院総合理工学府環境エネルギー工学専攻

2022

Master Thesis

# STEADY-STATE ANALYSIS OF DEW-POINT EVAPORATIVE COOLING SYSTEM

Interdisciplinary Graduate School of Engineering Sciences

Kyushu University

Department of Energy and Environmental Engineering

Thermal Energy Conversion System Laboratory

Yang Cheng

Supervisor Prof. Takahiko Miyazaki

Assoc. Prof. Kyaw Thu

Submit date 2022/02/07

# Abstract

This study focuses on learning the principle of dew point evaporative cooling system. A single-stage dew-point evaporative cooling system with counter-flow configuration was developed in this study by building numerical simulation model and experimental setup.

The evaporative cooling system was firstly designed by numerical simulation in terms of geometrical sizes and operating condition. The finite method was applied to make a solver in order to calculate the system equations, which can solve not only ordinary differential equations, but also partial differential equations. Python was the selected computer langrage to finish the whole calculation.

A small-scale dew point evaporative cooling system prototype was made in the laboratory which includes four main components: main m-cycle unit, water supply system, air supply system and measurement devices. The first purpose of building the experimental bench is to understand and learn the actual operation of the dew point evaporative cooler, and the second is to test the accuracy of the simulation model through actual experimental data. The results show that the error between the experimental data and the simulation results is about 15%. Which indicated that the current model was able to simulate the heat and mass transfer process in m-cycle cooling system.

Several operation conditions were carried with this validated numerical model and the system performance was manifested by wet-bulb and dew-point effectiveness. The numerical results indicate that the inlet condition (inlet air velocity and working ratio) and geometrical size (channel length and height) can have a significant effect on system performance. By changing the velocity from 1 m/s to 3 m/s, the wet bulb effectiveness can be changed from 1.38 to 0.96, while dew point effectiveness is from 0.88 to 0.62. Similarly, in the working ratio case, the wet bulb effectiveness is from 1.03 to 1.42, while dew point is from 0.66 to 0.91. For the geometrical case, increasing channel length brings the increasing of wet-bulb and dew-point effectiveness, when the channel length varies from 0.2 to 1.5m, the wet-bule effectiveness and dew-point effectiveness varies from 0.59 to 1.39 and 0.38 to 0.90.

# Contents

# Nomenclature

| | | |
|---|---|---|
| $A$ | area | $m^2$ |
| $c_p$ | specific heat | kJ/kg/K |
| $d$ | channel height | m |
| $D$ | mass diffusivity | $m^2/s$ |
| $D_h$ | hydraulic diameter | m |
| $k$ | thermal conductivity | kW/m/K |
| $L$ | channel length | m |
| $Nu$ | Nusselt number | - |
| $p$ | pressure | Pa |
| $Pr$ | Prandtl number | - |
| $RH$ | relative humidity | % |
| $Re$ | Reynolds number | - |
| $Sc$ | Schmidt number | - |
| $Sh$ | Sherwood number | - |
| $St$ | Stanton number | - |
| $St_m$ | Mass transfer Stanton number | - |
| $L_w$ | Lewis number | - |
| $T$ | temperature | °C |
| $t$ | time | s |
| $u$ | velocity | m/s |
| $x$ | Humidity ratio | g/kg [DA] |
| $dx$ | length | m |

Greek symbols

| | | |
|---|---|---|
| $\alpha$ | convective heat transfer coefficient | $W/m^2/K$ |
| $\alpha_m$ | mass transfer coefficient | m/s |
| $\varepsilon$ | effectiveness | - |
| $\lambda$ | coefficient of friction | - |
| $\nu$ | Kinematic viscosity | $(m^2)/s$ |
| $\rho$ | density | $kg/m^3$ |

Subscripts

| | |
|---|---|
| da | dry air |
| ds | channel plate (close to dry channel side) |
| wa | wet air |
| wsd | Water film |
| ws | Water surface |
| wb | wet-bulb |
| dp | dew-point |
| sat | saturation |

# Chapter 1 Introduction

## 1.1 Current World Energy Status

The electricity consumption for cooling with air conditioners and electric fans accounts for a portion of the residential electricity consumption. With the global warming trend, the rapidly growing population and the increasing demand for a comfortable living and working environment, the demand for cooling is also increasing, which is accompanied by increasing energy consumption and emissions.

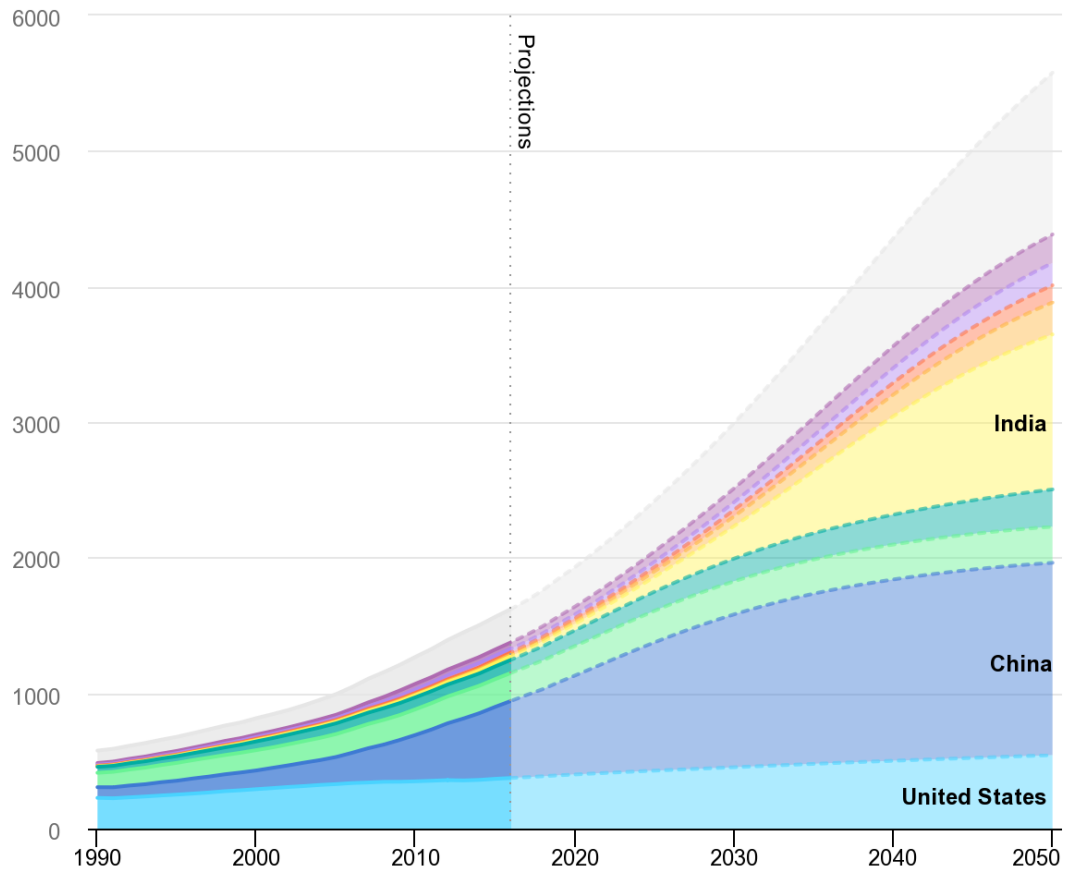


Fig.1.1 Global air conditioner stock.
IEA, Global air conditioner stock, 1990-2050, IEA, Paris https://www.iea.org/data-and-statistics/charts/global-air-conditioner-stock-1990-2050

From the perspective of population, it can be seen from the data map Fig.1.1 of IEA[1] that as a few countries with more population: India, China. The growing population demands more air-conditioning installations. The forecast shows that by 2050, India and China will account for about half of the world's installed air-conditioning capacity. Although the air-conditioning stock in the United States has not changed much compared with 2016, because it already has a large amount of air-conditioning stock in

the early years, the United States will still occupy a large share of the world in 2050.

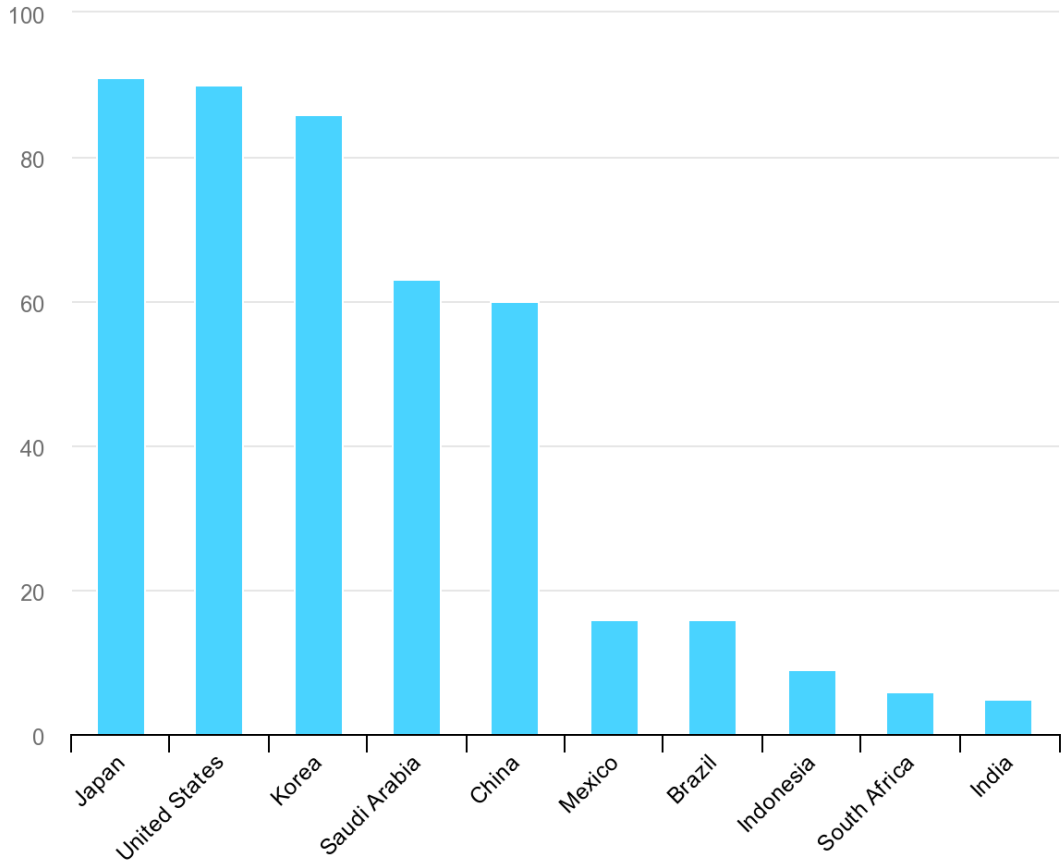


Fig.1.2 Percentage of households equipped with AC in countries.
IEA, Percentage of households equipped with AC in selected countries, 2018, IEA, Paris
https://www.iea.org/data-and-statistics/charts/percentage-of-households-equiped-with-ac-in-selected-countries-2018

From a climate perspective, here is another data graph from the IEA[1], which depicts the current state of household air conditioning holdings in various countries. From the Fig.1.2, it can be easily seen that although Japan, the United States, South Korea and other countries have high installed capacity, but countries in tropical regions such as Indonesia, South Africa and India, the holdings of household air conditioners in these places are relatively low. The demand for refrigeration in tropical regions is relatively high, therefore in the future, the rapid increase in the installed capacity of household air conditioners in tropical regions is foreseeable, which will pose a huge challenge to the world's energy problems.

Increasingly serious environmental issues and the continued increase in electricity consumption for cooling have brought more attention to new cooling methods because using efficient cooling is the easiest way to alleviate energy and emissions problems.

## 1.2 Air conditioning systems

### 1.2.1 Conventional vapor compression refrigeration system

As we know, the traditional mechanical vapor compression refrigeration system is composed of evaporator, condenser, compressor and expansion valve, and the refrigerant circulates in the device. As shown in the Fig.1.3, in the evaporator, the refrigerant absorbs heat from the environment and undergoes a phase change (from liquid to gas) to achieve the purpose of refrigeration. The vapor from the evaporator enters the compressor, and after consuming the electricity input from the outside, the gas is converted into high temperature and high-pressure, saturated vapor. This vapor then enters the condenser and releases heat to the environment through a phase change process (from gaseous to liquid). The liquid refrigerant leaves the condenser and enters the expansion valve, and is converted into a low-pressure gas-liquid coexisting fluid and returns to the evaporator to complete the entire refrigeration cycle. Because the traditional refrigeration cycle system has experienced hundreds of years of history, and has stable operation, low cost, long life and relatively good performance, it still occupies an absolute position in the air conditioning market. However, owing to the operation of the compressor requires additional input power, considering that the current power system is still dominated by thermal power generation, it is the general trend to explore and develop a high-efficiency refrigeration cycle.

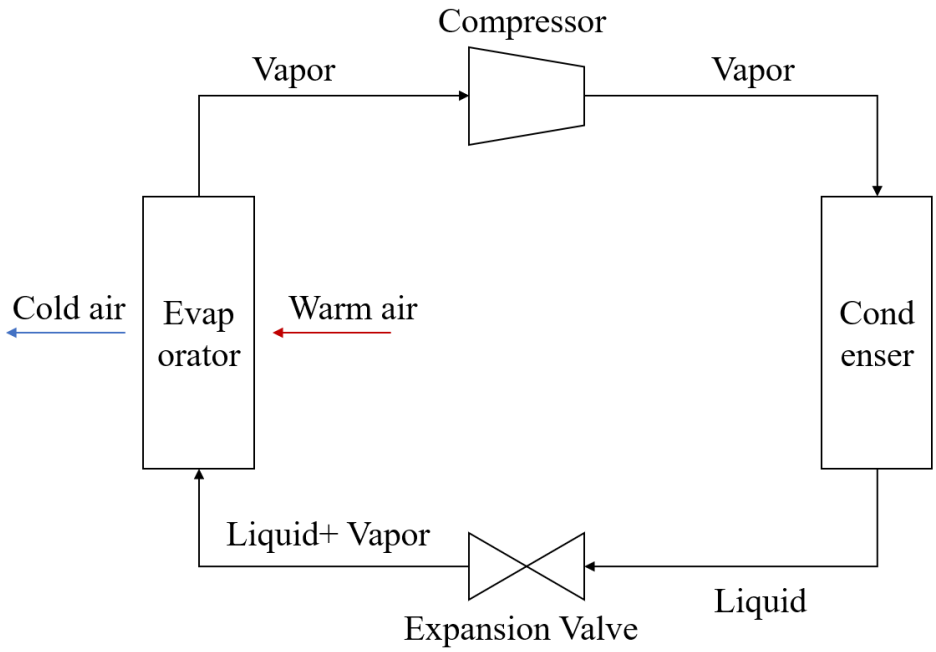


Fig.1.3 Basic traditional mechanical vapor compression refrigeration system

### 1.2.2 Evaporative cooling system

The principle of evaporative cooling is to use the vaporization phase change process of

water to absorb heat to achieve the purpose of refrigeration[2][3]. It has the advantages of simple structure (no compressor required), environmentally friendly (using latent heat of vaporization), and excellent performance. attracted the attention of researchers. Evaporative cooling is divided into direct evaporative cooling (DEC) and indirect evaporative cooling (IEC). The principle of direct evaporative cooling is shown in the Fig.1.4 (a), the high-temperature air directly enters the channel with the water layer, and the water layer absorbs the heat of the high-temperature air and evaporates to reduce the air temperature. However, the intake air is in direct contact with the water layer, which means that the air will obtain water vapor from the water layer through the evaporation process, which will cause the humidity of supply air becomes too high, which will cause an uncomfortable environment.

As an improved version of the direct evaporative cooling, the indirect evaporative cooling has another channel dedicated to the evaporation process, called the wet channel, as shown in Fig.1.4 (b). Intake air passes through the dry channel, while working air directly passes through the wet channel. The evaporation process in the wet channel causes the temperature of the channel plate to decrease. The temperature difference between the plate and the intake air is used to induce heat transfer between them, thereby achieving the purpose of cooling the intake air. In the process of indirect evaporative cooling, not only the temperature of the intake air is reduced, but the humidity does not change at the same time. Because of this advantage, it can be considered that the IEC has the potential to replace the traditional refrigeration system.

However, evaporative cooling also presents challenges. Evaporative cooling reduces the intake air to wet bulb temperature. In other words, the difference between the dry bulb temperature and the wet bulb temperature of the inlet air becomes a key factor affecting system performance. If the humidity of the inlet air is too high, it means that the dry bulb temperature is very close to the wet bulb temperature, which will greatly limit the cooling capacity of the system.

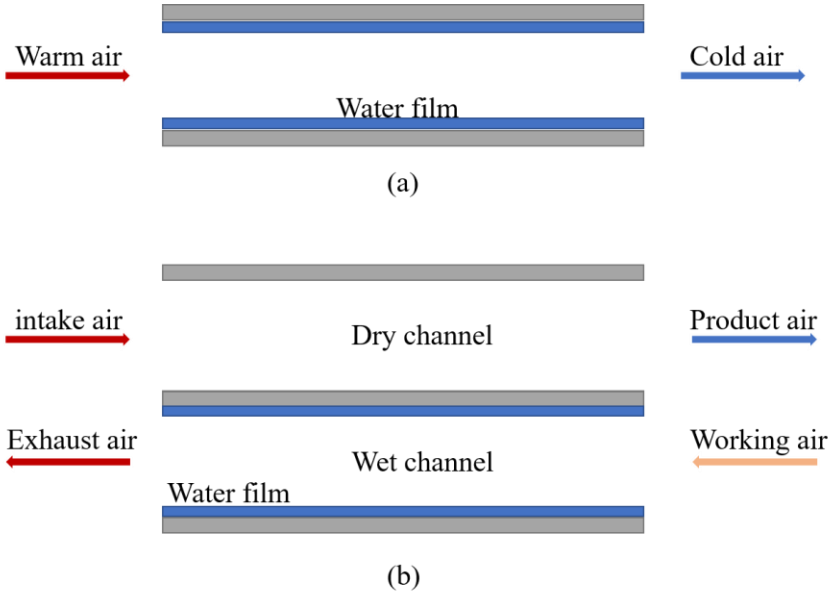


Fig.1.4 Evaporative cooling system. (a)DEC. (b)IEC.

## 1.3 Maisotsenko cycle

In recent years, a new type of indirect evaporative cooling system has been invented, which can reduce the intake air temperature to below the wet bulb temperature, close to the dew point temperature, as shown in Fig.1.5, known as dew point evaporative cooling, which is considered as a breakthrough in indirect cooling systems[4][5]. Therefore, it has received extensive attention from researchers and has developed rapidly.

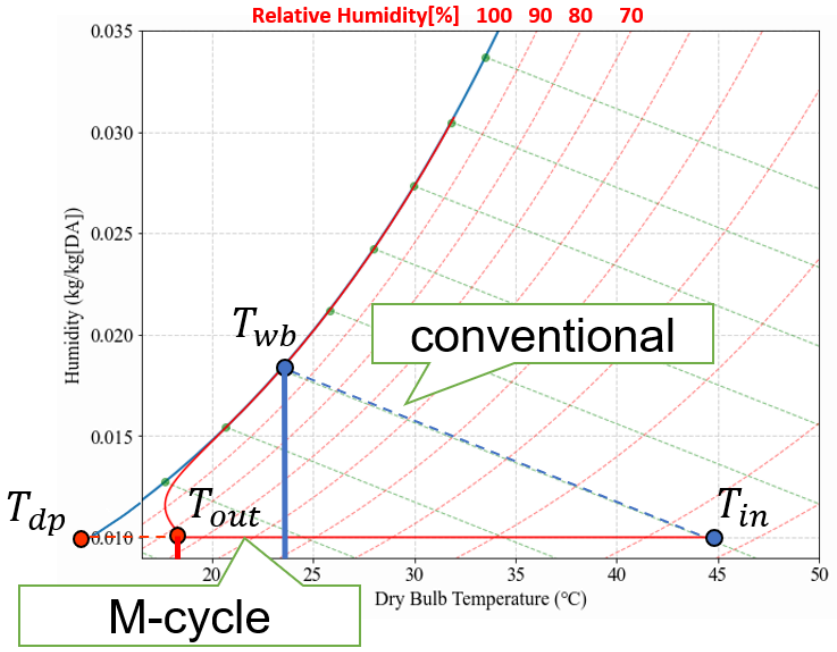


Fig.1.5 Comparison of conventional IEC and m-cycle cooling approach on psychrometric chart.

m-cycle was proposed by Professor Valeriy Maisotenko. The schematic diagram of the perforated cross-flow heat exchanger is shown in the Fig.1.6. First, the air is taken in into the dry channel, and a part of the air will directly pass through the entire dry channel and reach the outlet to become supply air. The other part of the air enters the wet channel through the holes in the plate and flows in the normal direction to the dry channel. During this process, the working air takes away the saturated water vapor of the water film and the heat from the dry channel, and then becomes high-temperature and high-humidity air and is released into the environment, while the intake air continuously loses heat in the dry channel and exits at the outlet. It becomes supply air with low humidity and temperature below wet bulb temperature, close to dew point temperature.

Although the cross-flow m-cycle system has achieved better efficiency than conventional evaporative cooling, this article points out that the cross-flow m-cycle heat exchanger can achieve a wet bulb efficiency greater than 81% and a dew point greater than 50% efficient[6]. However, the premature entry of the working air into the

wet channel results in a small temperature difference between the air and the channel plate, which limits system performance.

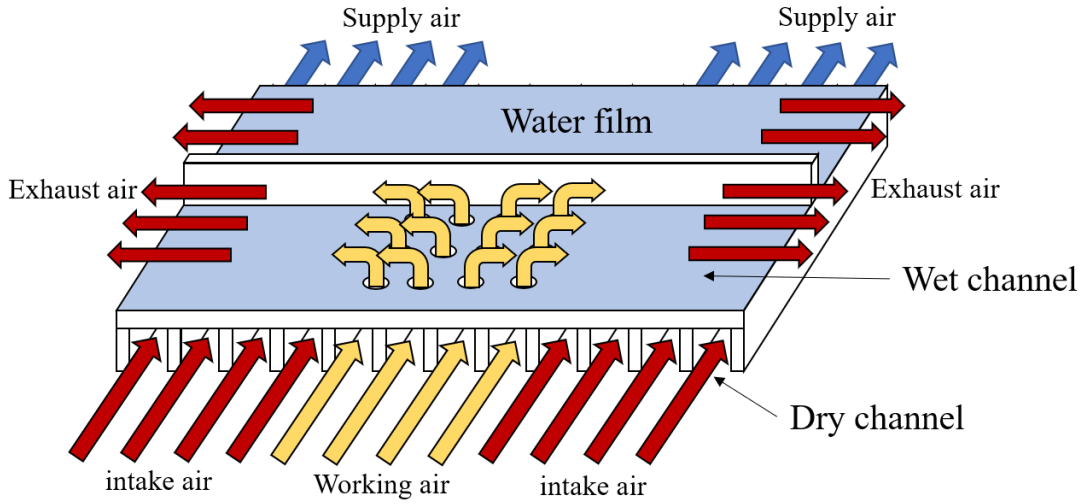


Fig.1.6 schematic of cross-flow based m-cycle module.

In order to further improve the cooling efficiency and optimize the problem of the cross-flow m-cycle system, a counter-flow m-cycle cooling system is proposed[7], and its principle is shown in the Fig.1.7. Unlike the cross-flow holes opening position (along the air flow direction of the dry channel), the counter-flow hole is opened at the end of the dry channel. Based on this structure, the intake air first passes through the dry channel, and a part of the air at the end is directly released into the room as supply air, another part of the air enters the wet channel as working air. Different from cross-flow, the temperature of the working air entering the wet channel is also close to the dew point temperature, and the temperature difference between the channel plate and the working air is large, which is beneficial for the heat and mass transfer processes in the wet channel. Both simulation and experiment show that the counter-flow dew point evaporative cooling system has better wet bulb and dew point efficiencies than cross-flow one.

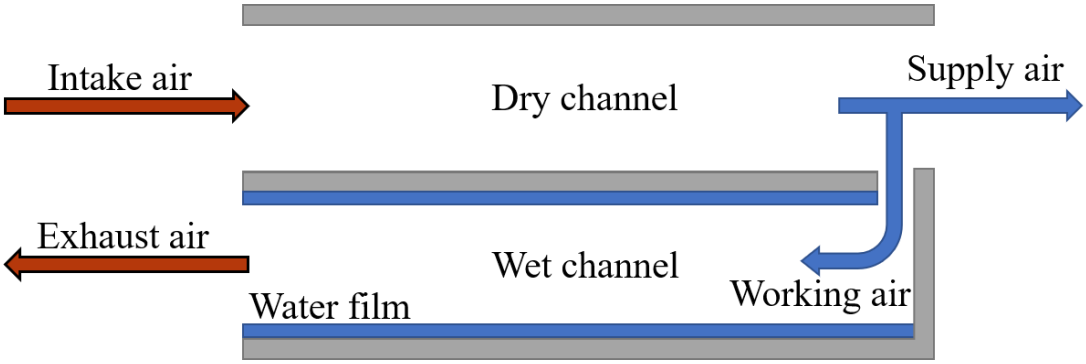


Fig.1.7 schematic of counter-flow based m-cycle module.

## 1.4 Current status of M-cycle technology

Many studies on dew point evaporative cooling systems have been published, mainly focusing on analyzing the heat and mass transfer process between channels, evaluating the performance of the system, and analyzing the effects of different structures, materials, and operating conditions on the system. A summary of the study and achievement is shown below.

### 1.4.1 Simulation

Table 0.1 Simulation model

| author | Heidarinejad et al. [8] | Anisimov et al. [9][10][11] | Pandelidis et al. [12] | Hasan [13][14] | J. Lin[15] |
|---|---|---|---|---|---|
| Flow path | Cross-flow | Cross-flow | Counter-flow | Counter-flow | Counter-flow |
| Inlet data | | | | | |
| Inlet temperature (℃) | 35.5 | 25 - 45 | 30 | 30 | 25- 45 |
| Inlet humidity (g/kg [DA]) | 22 | RH 20%-60% | RH 40% | RH 34% | 3-18 |
| Inlet velocity (m/s) | - | 1.8-7.0 | 3.0 | 0.68 | 0.5-3.5 |
| Channel length (m) | - | 0.25-1.0 | 0.5 | 0.5 | 0.6-2.0 |
| Channel height (mm) | 7 | 2.5-20 | 30 | 3.5 | 3-8 |
| Validation | Compare with published experimental data | Against experimental data from literature | Against existing experimental data | Experimental measurements available in the literature | With several published experimental data |
| Features | Discretized using finite difference method and solve by iterative method. | Numerical model is developed based on a modified e-NTU method | One-dimensional heat and mass transfer model based on a modified e-NTU method | Modified e-NTU method: linear slope for saturation temperature-enthalpy relation of air | Finite difference method and solve by the Newton Raphson iteration method using MATLAB |

| author | X. Zhao et al. [7] | Changhong Zhan et al. [16] |
|---|---|---|
| Flow path | Counter-flow | Cross-flow |
| Inlet data | | |
| Inlet temperature (℃) | 28 | 30 |
| Inlet humidity (g/kg [DA]) | - | RH 50% |
| Inlet velocity (m/s) | - | - |
| Channel length (m) | - | - |
| Channel height (mm) | - | - |
| Validation | - | Against experimental data from literature |
| Features | solve by the Newton iterative method taken from EES software, equilateral-triangle-shaped grids | Using finite-element method by EES |

As shown in the table above, many studies focus on establishing correct and appropriate mathematical models, mainly in one-dimensional models. Most of the simulation models are validated using published experimental data.

### 1.4.2 Experiment

Table 0.2 Experiment

| author | B. Riangvilaikul and S. Kumar [17] | Pacific Gas and Electric Company [6] | Z. Duan[18] | Changhong Zhan et al. [19] | M. Jradi and S. Riffat[20] |
|---|---|---|---|---|---|
| Flow path | Counter-flow | Cross-flow | Counter-flow | Cross-flow/counter-flow | Cross-flow |
| Inlet data | | | | | |
| Inlet temperature (℃) | 25-45 | 26.7-43.8 | 25-45 | 28 | 25- 43 |
| Inlet humidity (g/kg [DA]) | 7-26 | - | 6.9-26.4 | 11.35 | RH 34-71% |
| Intake air velocity (m/s) | 2.4 | - | 0.5-1 | - | 1.75-3.5 |
| Channel length (m) | 1.2 | - | 2 | 1 | 0.1-0.8 |
| Channel height (mm) | 7 | - | 3-6 | 5 | 1-15 |
| Wick material | Cotton sheet coated with polyurethane | - | Rough/smooth surface of textile fibre; Pure/waxing kraft paper; Non-woven fabric; Aluminum film | Fibre with water-proof | Fibrous material |
| Measured data | Temperature Humidity ratio Velocity at inlet and outlet of system | Air flow rate dry bulb, dew point temperature pressure power consumption water flow rate fan speed | Dry bulb, wet bulb temperature Humidity ratio RH Air velocity | Dry bulb, wet bulb temperature Humidity ratio RH Air velocity | Temperature Humidity ratio Velocity at inlet and outlet of system |
| Simulation model | No | No | yes | yes | yes |

| author | J. Lee and D. Lee[21] | F. Bruno[22] | Ali Pakari and Saud Ghani [23] |
|---|---|---|---|
| Flow path | Counter-flow | Counter-flow | Counter-flow |
| Inlet data | | | |
| Inlet temperature (℃) | 27.5-32 | 27.5-40.4 | 30-45 |
| Inlet humidity (g/kg [DA]) | 9.19-18.11 | - | RH 40% |
| Intake air velocity (m/s) | - | - | - |
| Channel length (m) | 0.35 | - | 0.2-0.6 |
| Channel height (mm) | 20(dry)/10(wet) | - | 300 |
| Wick material | - | special medium with the characteristics of high-water retention and wick ability | Wick paper |
| Measured data | Temperature<br>Humidity ratio<br>Velocity | Temperature<br>Humidity ratio<br>Velocity | Dry bulb, wet bulb temperature<br>Humidity ratio<br>RH<br>Air velocity |
| Simulation model | yes | No | yes |

The above table is the experimental part of the dew point evaporative refrigeration system, which aims to test the influence of different working conditions and different initial conditions on the system. Part of the work is only doing experiments, and the other part of the work establishes a simulation model and an experimental bench at the same time.

## 1.5 Purpose of this study

More on dew point evaporative cooling systems are summarized in this paper[24]. In conclusion, compared to using published experimental data to validate the simulation model, building a test bench can better learn the m-cycle in real operating conditions. The performance of the cooling system, and after verifying the simulation model through experimental data, the comparison data can propose influencing factors, so that the simulation model can better simulate the performance of the dew point evaporative cooling system in real life. Therefore, this study has two main purposes:

1. To establish a mathematical model, and apply a simplified conditions to complete the system equations in steady state. Calculate ordinary differential equations in Python using Powell's method. This method can solve not only ordinary differential equations, but also partial differential equations, which can prepare for subsequent combined adsorption and desorption.[25]

2. Complete and test a small-scale dew point evaporative cooling system prototype in the laboratory, determine the geometry, wick material, water supply system, air supply system, sensors and measuring points.

This study consists of the following parts:
Chapter 2 introduces the establishment of system equations and how to implement them in Python.
Chapter 3 introduces the establishment of the prototype of the m-cycle system test bench.
Chapter 4 introduces and analyzes the results of the simulation model in Chapter 2.
Chapter 5 summarizes the full thesis.

# Chapter 2 Configuration and calculation of dew-point evaporative cooling system

In this chapter, it will be introduced in detail how to build the mathematical model and the method for solving ordinary differential equations, how to write the mathematical model into the simulation program.

## 2.1 description of dew-point evaporative cooling system

A single-stage dew-point evaporative cooling system with counter-flow configuration is shown as Fig.2.1, which contains two groups of channels, each group contains a dry channel and a wet channel; and the inlet and outlet contain three airflows: (1)intake air; (2)supply air; (3) working air. High temperature and low humidity intake air enters the dry channel from the environment, heat conduction occurs due to the temperature difference between the dry air and channel plate, which has lowered the temperature of the intake air. When the air leaves the dry channel, a part of the air is directly supplied to the environment called supply air; the other part of the air will enter the wet channel as working air. The evaporation process occurs in the wet channel due to the difference in humidity between the working air and the saturated water vapor near the water film; the heat required for this process is obtained from the adjacent dry channel. Therefore, based on the above thermodynamic process, the supply air leaving the dry channel can be cooled to approach the dew-point temperature, which is also the difference between the m-cycle based evaporative cooling system and the conventional evaporative cooling system.

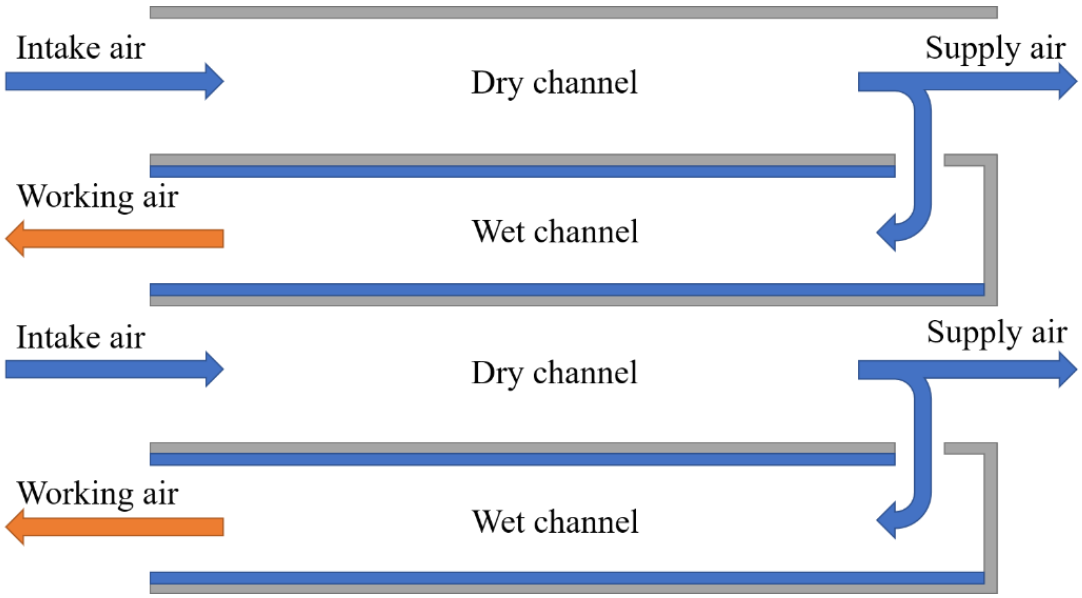


Fig.2.1 schematic diagram for a single-stage dew-point evaporative cooling system

## 2.2 Mathematical model

Reference to published works[26][15][27], before building the system of equations, first we divide the channel into many identical elements. In each element there are control volumes for the dry channel, the wet channel and the channel plate, water film, as shown in Fig.2.2, containing half the dry channel, the channel plate and water film, and half the wet channel.

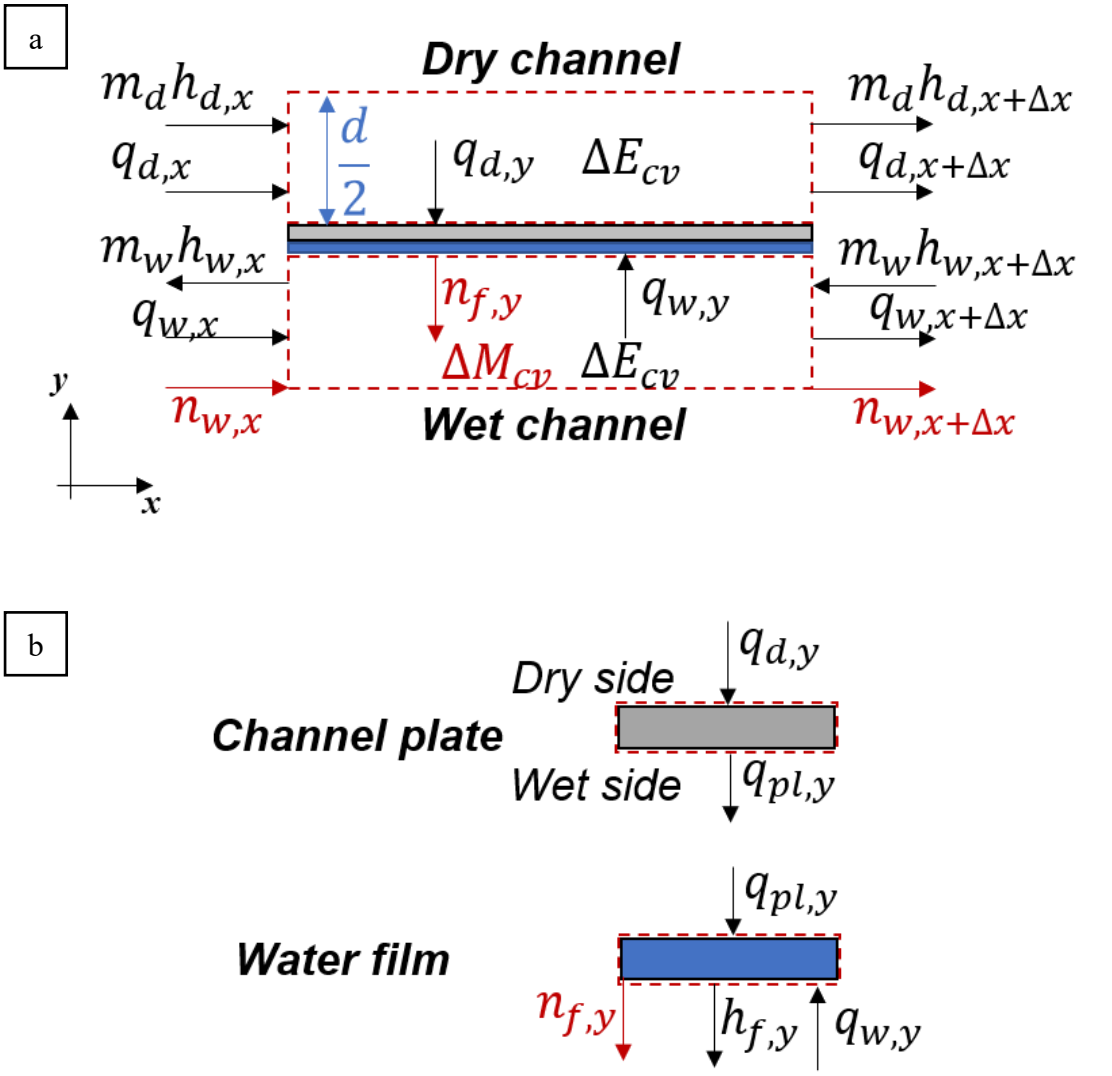


Fig.2.2 different control volume (red dotted line) for: (a)dry channel, wet channel, (b) channel plate and water film

A transient model has been built based on the following general assumptions:

a) Adiabatic conditions between channel unit and surrounding circumstance.
b) Water film inside the wet channel is saturated and stagnant.
c) Air density around the dry channel is constant.
d) The properties are uniform within the control volume.
e) The advection term is neglected.

Based on the energy balance of air in the control volume, the following temperature calculation equations can be given:

1) Dry channel:

$$\rho c_v \frac{\partial T_{da}}{\partial t}\frac{d}{2} = k\frac{d^2 T_{da}}{dx^2}\frac{d}{2} + \alpha_{da}(T_{ds} - T_{da}) - \rho c_p u_{da}\frac{\partial T_{da}}{\partial x}\frac{d}{2} \quad (1)$$

at steady state, the transient term is neglected and the equation becomes:

$$\rho c_p \left(u_{da}\frac{\partial T_{da}}{\partial x}\right)\frac{d}{2} = \alpha_{da}(T_{ds} - T_{da}) \quad (2)$$

Where the right-hand side term indicates the convective heat transfer between the dry air and channel plate surface (dry side).

2) Wet channel:

In the wet channel, both heat and mass transfer occur therefore based on the energy balance and mass balance, equations for working air can be given as:

$$\rho c_v \frac{\partial T_{wa}}{\partial t}\frac{d}{2} = k\frac{d^2 T_{wa}}{dx^2}\frac{d}{2} + \alpha_{wa}(T_{wsd} - T_{wa}) - \rho c_p u_{wa}\frac{\partial T_{wa}}{\partial x}\frac{d}{2} \quad (3)$$

$$\frac{\partial \rho_{wa}}{\partial t}\frac{d}{2} = D_{wa}\frac{d^2 \rho_{wa}}{dx^2}\frac{d}{2} + \alpha_m(\rho_{ws} - \rho_{wa}) - u_{wa}\frac{\partial \rho_{wa}}{\partial x}\frac{d}{2} \quad (4)$$

Under the steady state, the differential equations can be converted into:

$$\rho c_p \left(u_{wa}\frac{\partial T_{wa}}{\partial x}\right)\frac{d}{2} = \alpha_{wa}(T_{wsd} - T_{wa}) \quad (5)$$

$$\left(u_{wa}\frac{\partial \rho_{wa}}{\partial x}\right)\frac{d}{2} = \alpha_m(\rho_{ws} - \rho_{wa}) \quad (6)$$

Where the right-hand side of Eq. stand for the convective heat transfer between the dry air and channel plate surface (wet side), and about Eq. the right-hand side term denotes the mass transfer between the working air and saturated air near the water film due to the different water vapor density.

3) Channel plate and water film:

The temperature of channel plate and water film is calculated by considering the temperature difference between the air and plate. In this case, the temperature of channel plate (wet side) is same as the water film. The heat flux of dry air, channel plate and wet air are given as:

$$q_{dry} = \alpha_{da}(T_{da} - T_{ds}) \tag{7}$$

$$q_{wall} = \frac{k(T_{ds} - T_{wsd})}{d_p} \tag{8}$$

$$q_{wet} = \alpha_{wa}(T_{wsd} - T_{wa}) + L_w\alpha_m(\rho_{ws} - \rho_{wa}) \tag{9}$$

The Eq. represents the convective heat transfer from dry channel while the Eq. indicates the longitudinal heat conduction between the dry and wet side of the channel plate. The Eq. denotes the convective heat transfer from wet channel and latent heat transfer by water evaporation.
By applying the energy balance, the expressions for the surface temperature are given as:

$$q_{dry} - q_{wall} = 0 \tag{10}$$

$$q_{wet} - q_{wall} = 0 \tag{11}$$

In the above model, 5 variables can be calculated, namely the air temperature of the wet and dry channel, the water vapor density of the wet air (used to calculate the humidity ratio) and the temperature of the channel plate surface.

4) Performance evaluation:
The wet-bulb effectiveness and dew-point effectiveness are two parameters commonly used to measure system performance of evaporative cooling system, which is expressed as:

$$\varepsilon_{wb} = \frac{T_{dry,inlet} - T_{dry,outlet}}{T_{dry,inlet} - T_{wet-bulb,inlet}} \tag{12}$$

$$\varepsilon_{dp} = \frac{T_{dry,inlet} - T_{dry,outlet}}{T_{dry,inlet} - T_{dew-point,inlet}} \tag{13}$$

5) Parameter
In this mathematical model, inlet effects are not considered, so the Nusselt number is set to a constant value equal to 7.45.[28] and the function of computing diffusion is given as:
When the temperature is less than 80℃:

$$D = 104.91143 \times 10^{-6} \times Current\ Temperature^{1.744} / Current\ Pressure \quad (14)$$

Else:

$$D = 805.2375 \times 10^{-6} / Current\ P \times (Current\ T)^{\frac{5}{2}} / (Current\ T + 190) \quad (15)$$

For the calculation of Lewis number, which is used for calculate the latent heat, the function is expressed as:

$$Lw = 4185.5 \times (751.78 - 0.5655 \times Current\ surface\ Temperature) \quad (16)$$

For the pressure drop through the channel, by applying Darcy-Weisbach Equation:

$$\lambda = \frac{64}{Re} \quad (17)$$

$$\Delta p = \lambda \frac{\Delta z}{D_h} \frac{\rho u^2}{2} \quad (18)$$

Since the density of water vapor in the working air varies in the wet channel, how to obtain the water vapor density from pressure and temperature is one of the most important parameters in this model. The density of water vapor in working air can be calculated by the following empirical formula:
Partial pressure:

$$p_{part} = \frac{p_{total} \cdot x}{(0.018015268 / 0.02896546 + x)} \quad (19)$$

Where $x$ represents the current humidity ratio of air and $P_{total}$ is the total pressure. And the constant value of 0.018015268 and 0.02896546 is the molar value of water and dry air.
And the vapor density of working air can be calculated by using partial pressure:

$$\rho_{vapor} = \frac{p_{part}}{T} . 0.018015268 / 8.314462175 \quad (20)$$

Where $T$ is the current dry-bulb temperature of working air.
Calculation of the saturation pressure:
When the temperature is less than 0℃,

$$p_{sat} = \exp\left(\frac{c1}{T} + c2 + c3 \cdot T + c4 \cdot T^2 + c5 \cdot T^3 + c6 \cdot T^4 + c7 \cdot \log(T)\right) \quad (21)$$

Else,

$$p_{sat} = \exp\left(\frac{c8}{T} + c9 + c10 \cdot T + c11 \cdot T^2 + c12 \cdot T^3 + c13 \cdot \log(T)\right) \quad (22)$$

Where c1 = -5674.5359, c2 = 6.3925247, c3 = -0.009677843, c4 = 0.00000062215701, c5 = 2.0747825e-09, c6 = -9.484024e-13, c7 = 4.1635019, c8 = -5800.2206, c9 = 1.3914933, c10 = -0.048640239, c11 = 0.000041764768, c12 = -0.000000014452093, c13 = 6.5459673.
Converting density into humidity ratio:

$$RH = \frac{p_{part}}{p_{sat}} \quad (23)$$

$$x_{wa} = \frac{0.018015268}{0.02896546} \cdot RH \cdot \frac{p_{sat}}{(p_{total} - RH \cdot p_{sat})} \quad (24)$$

## 2.3 Simulation scheme

Numerical simulation is based on the government equations of Eq. Before writing the code, some simplifications have been done below:
Temperature and density calculation
take dry air temperature Eq. as an example, the Eq. can be converted into:

$$\frac{\partial T_{da}}{\partial x} = \frac{\alpha_{da}}{\rho c_p u_{da}} (T_{ds} - T_{da}) \frac{2}{d} \quad (25)$$

While

$$\frac{\alpha_{da}}{\rho c_p u_{da}} = \frac{\frac{\alpha_{da} d}{k}}{\frac{\rho u_{da} d}{\nu} \cdot \frac{\nu c_p}{k}} = \frac{Nu}{RePr} = St_d \quad (26)$$

Therefore, by using the Stanton number, the following final form can be obtained:

$$0 = \left(T_{da} - T_{da\_old}\right) - \left(\frac{2}{d} St_d (T_{ds} - T_{da})\right) dx \tag{27}$$

Similarly, wet air temperature equation becomes:

$$0 = \left(T_{wa} - T_{wa\_old}\right) - \left(\frac{2}{d} St_w (T_{wsd} - T_{wa})\right) dx \tag{28}$$

For the density equation, by using mass transfer Stanton number, Schmidt number and Sherwood number: $St_m = Sh/(ReSc) = \alpha_m/u_{da}$, the Eq. becomes:

$$0 = \left(\rho_{wa} - \rho_{wa\_old}\right) \frac{\alpha_m}{u_{wa}} (\rho_{ws} - \rho_{wa}) \frac{2}{d} \tag{29}$$

Parameter calculation

Although some air parameters such as density, specific heat, viscosity, and thermal conductivity can be calculated using formulas, at the simulation level, there is an easier way to obtain these values, which is to use libraries in python to obtain these values directly. For the humid air, a library called HumidAirPropsSI can be imported into the program and give the value the program needs automatically. For the Lewis number, the value can be easily obtained by using the enthalpy difference (provided by python library called CoolPropsSI) between the liquid and gas phases of water. The parameter that related to the water vapor can be obtained from library CoolPropsSI by setting the gas phase.

The ordinary differential equations are solved by Powell's method in the Python environment. The spatial grid size is set at 0.09m and 100 cells along the channel. The follow boundary conditions were used in the simulation.

1) Inlet conditions for dry channel

The initial temperature and humidity ratio of dry air are equal to the given initial value.

$$T_{da}(0) = T_{da,inlet}\ , x_{da}(0) = x_{da,inlet} \tag{30}$$

Where the humidity ratio can be converted into vapor density when inputted into calculation.

2) Inlet conditions for wet channel

The initial temperature and humidity ratio of wet air are equal to the final value of dry air.

$$T_{wa}(L) = T_{da}(L)\ , x_{wa}(L) = x_{da}(L) \tag{31}$$

3) Inlet condition for channel plate and water film

The guess value of channel plate and water film are given as constant value and the temperature of water film value is lower than the temperature of wet air.

Since the inlet conditions for all variables are given value, the forward difference was adopted. While the inlet conditions for wet channel is given at the end of the channel (L), therefore the backward difference was applied to calculate both temperature and vapor density inside the wet channel. As shown in Fig.2.3

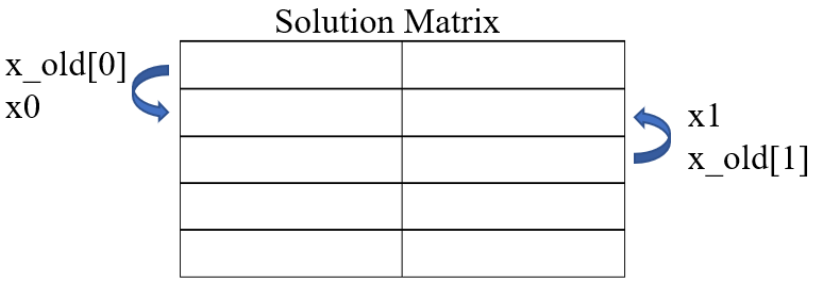


Fig.2.3 backward difference, forward difference schematic

The complete calculation has the following steps:

1. Setting the initial value for variables (Temperature of air, Temperature of surface and water film, inlet humidity ratio for dry air, pressure).
2. Define a guess vector with initial value.
3. Define a solution matrix and initialize the matrix with guess value.
4. Copy the solution matrix as a temporary matrix.
5. Input the first solution matrix into solver and get the result.
6. Update the solution matrix with the result in step5, called second solution matrix.
7. Calculate the difference between second solution matrix and temporary matrix, if the error is less than a certain value, output the result as the final solution matrix.
8. If the error does not satisfy the condition, then input the current solution matrix into solver and update the temporary matrix with the current solution matrix.

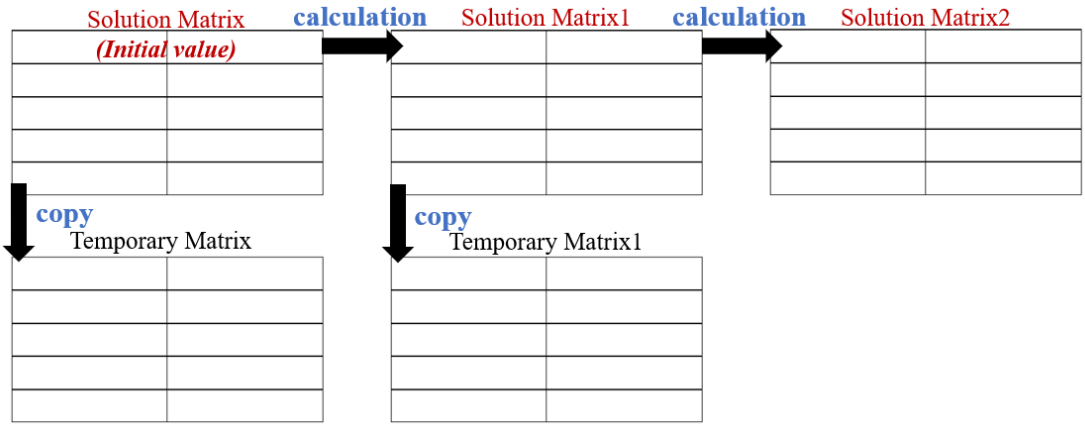


Fig.2.4 solution and temporary matrix update schematic

The detail of the simulation running process is illustrated by the chart given below.

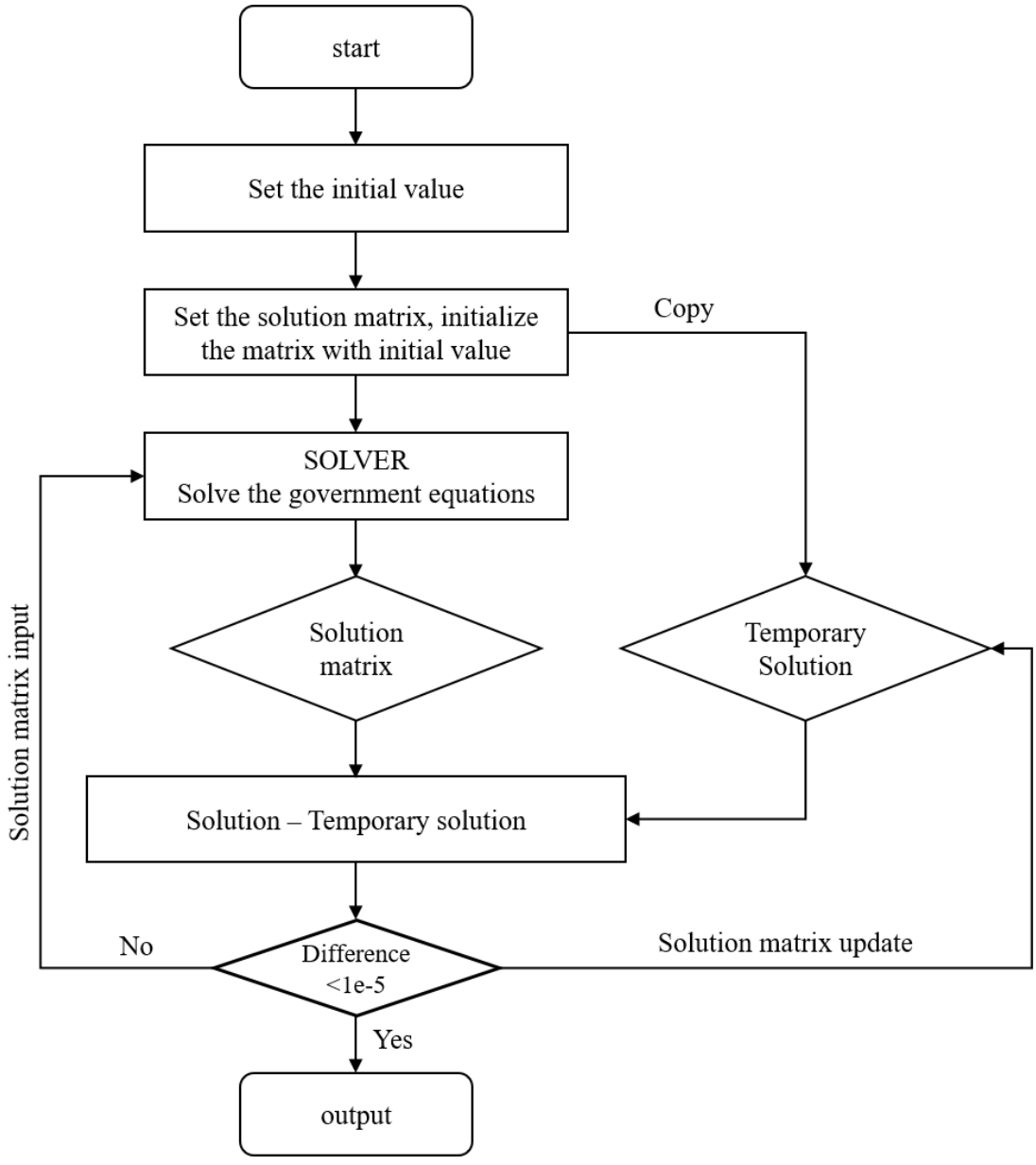


Fig.2.5 system equations calculation flow

# Chapter 3 Experimental validation of the model accuracy

## 3.1 Basic information of the m-cycle experimental unit

Currently a prototype set of experiment was made to validate the model accuracy. In order to compare the experimental and simulation results, the geometric parameters used in the simulation are consistent with the elements in the experiment.

Fig.3.1 Completed M-cycle counter-flow heat exchanger

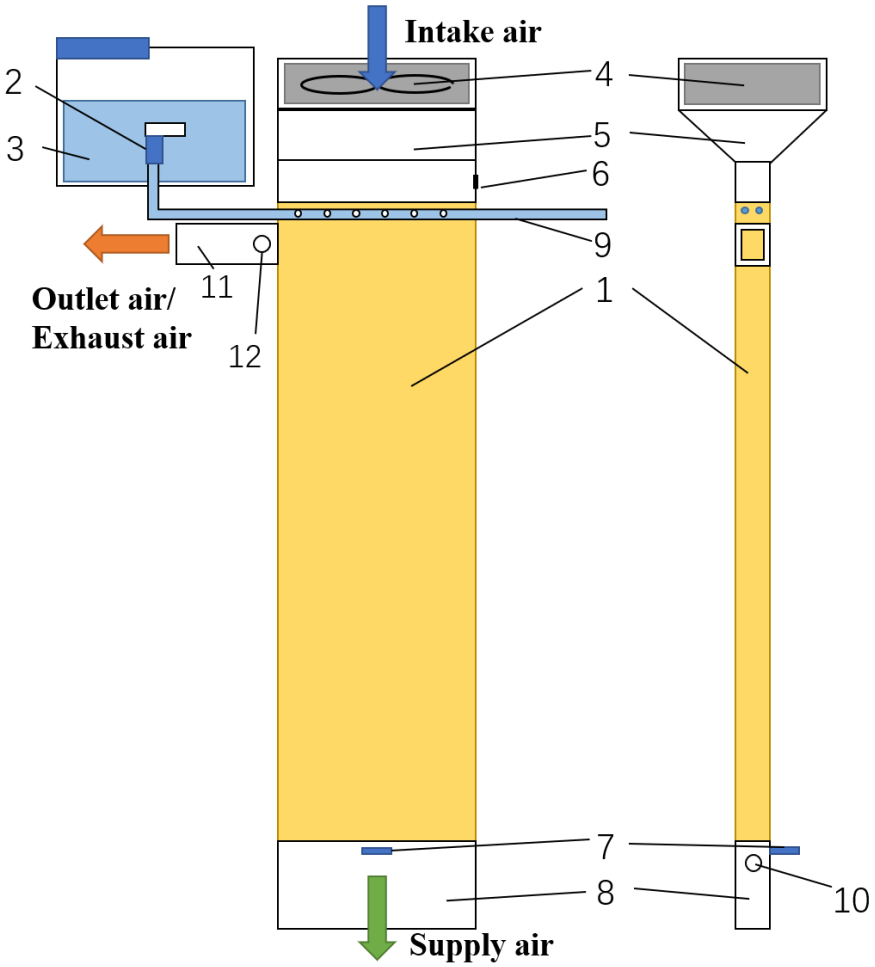


Fig.3.2 counter-flow based air cooler

The design of the prototype M-cycle counter-flow cooling system was shown schematically in Fig.3.2 The system mainly consists of four parts: (1)water supply, which includes a water tank(No.3) with a valve(No.2) and a soft rubber tube(No.9); (2)air supply, completed by a desktop cooling fan (No.4), Other parts are the handle of the grille(No.7) to control the working ratio and the duct(No.8 and No.11) to reduce the influence of the outlet, and the inlet duct(No.5) to place the fan.; (3)M-cycle unit/dew-point heat and mass exchanger(No.1) and (4)measuring part, which consists of three test point(No.6, No.10 and No.12).

The system consists of 2 dry channels and 2 wet channels (shown in Fig.3.3) and was externally insulated to reduce heat loss and air leakage.

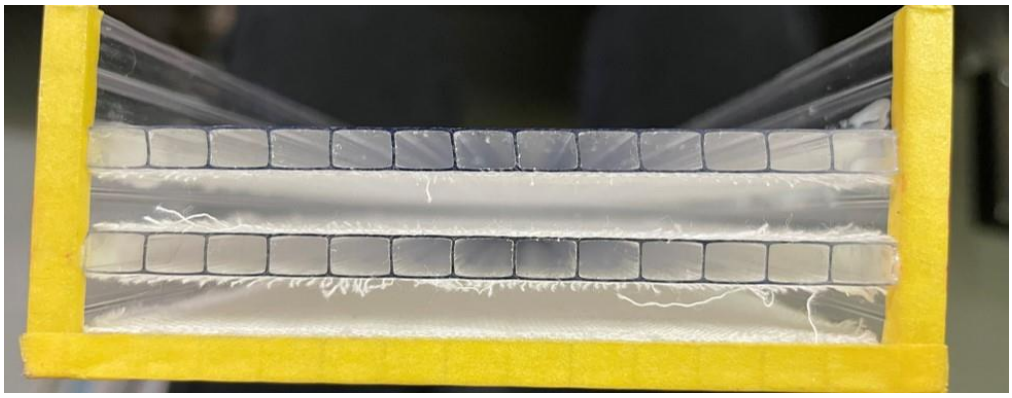

Fig.3.3 Channel composition of m-cycle unit

1) Water supply:

In order to ensure that the water layer in the wet channel is always in a saturated state, it is necessary to provide moisture to the wick material in the wet channel. In this case, as shown in Fig.3.4, the units are placed vertically, using gravity to provide moisture from top to bottom, a soft rubber tube is inserted directly into the wet channel (near the air inlet), and small holes are drilled on both sides of the tube, so that moisture can be supplied to the wick material on both sides at the same time. Water is provided by a 20 L tank with a valve.

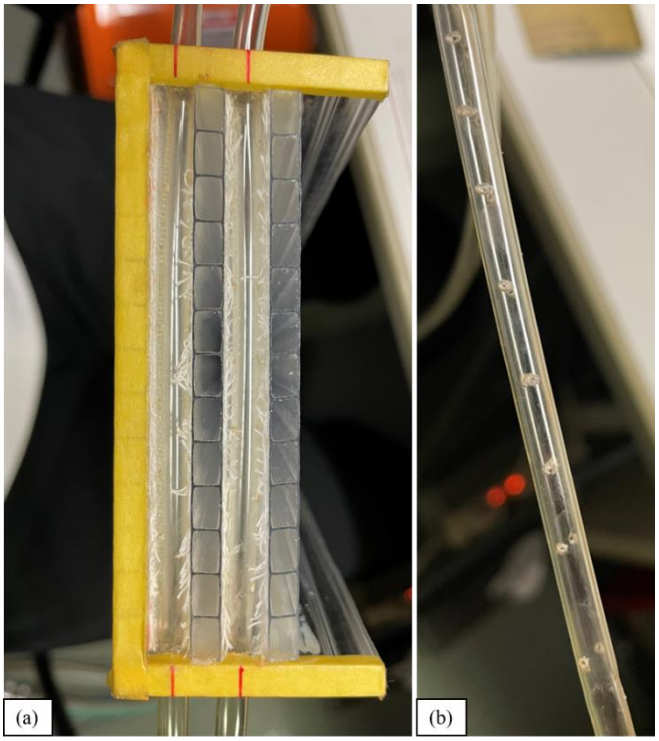


Fig.3.4 water supply (a)view of top side. (b)holes on the tube.

2) Air supply:

For the prototype unit, due to the small inlet area of the dry channel, a large volume flow is not required. Therefore, air is supply by a pc fan (SilverStone FN81) which can

provide maximum 0.72$m^3$/MIN. Inlet air velocity is controlled by a variable DC power supply, which the air velocity spans 0.1-1.8m/s. The main unit is built based on the counter-flow. The specific flow path is shown in Fig.3.5:

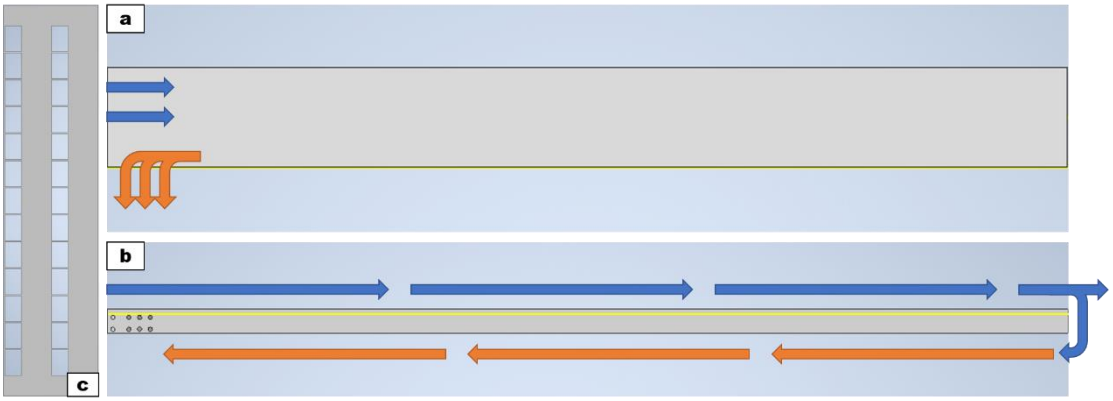


Fig.3.5 Three view of the m-cycle unit (a)Top view. (b)Main view. (c)Left view. (Air inlet)

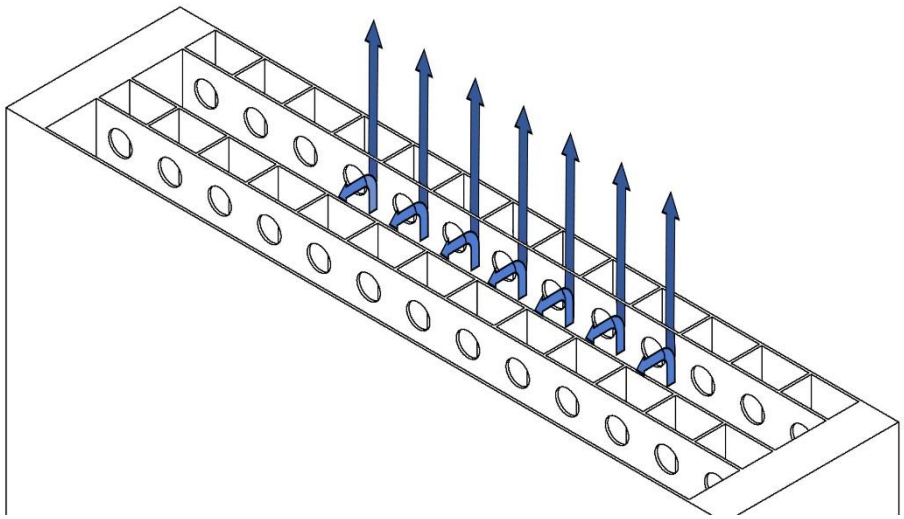

Fig.3.6 Schematic diagram of the bottom air path

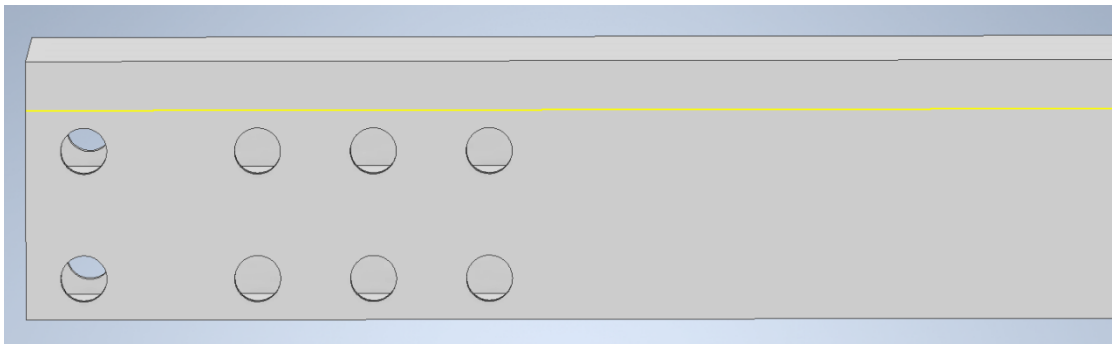

Fig.3.7 Air outlet details, the two through holes on the left are for inserting water supply tubes, and the six holes on the right are working air outlets.

Firstly, the air enters the unit from the dry channel, and the entrance of the wet channel

is completely block. The air passes through the dry channel, and some holes are drilled at the bottom of the dry channel, as shown in the Fig.3.6, at this position, a part of the air directly leaves the dry channel and enters the environment, which is called supply air, and the other part of the air enters the wet channel through the holes and is called working air. Since the top of the wet channel is completely closed, the outlet of the working air is set on the side of the unit. As shown in Fig.3.7, six holes are opened on the side of the unit.

3) M-cycle main unit:

Table 1 shows the basic specifications of the parameters used in this experiment, The wick material is used to simulate the water layer in the wet channel, which is used to provide moisture to the air. 100%Cotton sheet is selected in this case because it has the advantages of good water absorption ability, easy availability and affordable price.

Polycarbonate was selected as the material to build the whole system owing to its excellent thermal insulation properties, the water absorption rate is 0.17%. As mentioned in the calculation section, in the system equation, the advection terms need to be ignored to ensure the validity of the calculation, which means that the channel material needs to have a low thermal conductivity, which is the reason for this material.

For the working ratio, in this case, since the area of the inlet and outlet is inconsistent, we use the inlet and outlet volume flow to calculate the working ratio instead of the velocity. The specific calculation formula is as follows:

$$working\ ratio = \frac{v_{outlet} \times A_{outlet}}{v_{inlet} \times A_{inlet}} \tag{32}$$

Among them, the inlet and outlet area are a known quantity, the inlet and outlet velocity can be measured by the velocity sensor, and based on the above data, the working ratio can be calculated.

In this experiment, the bottom of the wet channel is 100% closed, and we control the working ratio by manually pushing and pulling the grille, as shown in the Fig.3.8.

Table 3.1: Basic specifications of the parameters used in experiment.

| Parameters | Specification/Values |
|---|---|
| Wick material | 100%Cotton sheet |
| Wall material | Polycarbonate |
| Wall thickness(mm) | 0.45 |
| Channel length(m) | 0.9 |
| Channel width(mm) | 83 |
| Channel height(mm) | 4.5 |
| Working ratio | 0.1-1.0 |

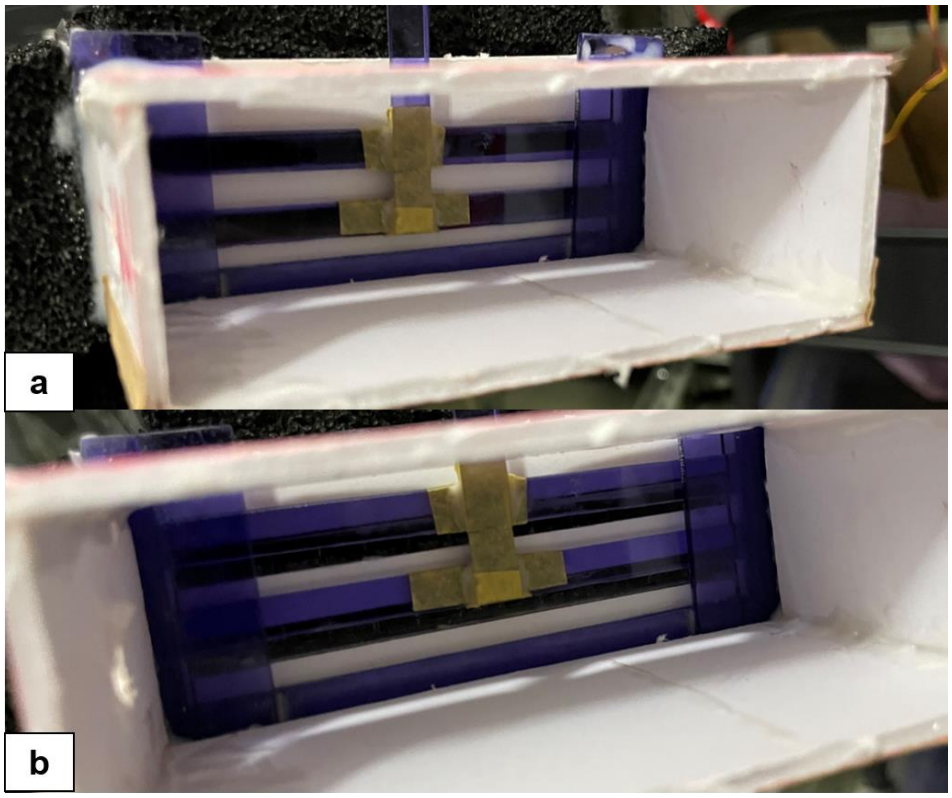


Fig.3.8 working ratio control device. (a)100% closed; (b)partly open

4) Measurement device:

A handheld Thermo-Anemometer (testo 405i) measured the air velocity. Temperature and humidity ratio are measured by Thermo-Hygrometer testo 605i.

Table 3.2: Specification of measuring devices.

| Instruments | Model | Parameters | Measurement range | Accuracy |
|---|---|---|---|---|
| Thermo-Hygrometer | Testo 605i | Temperature (℃) | -20 to +60℃ | ±0.8℃ (-20 to 0℃)<br>±0.5℃ (0 to 60℃) |
| Thermo-Hygrometer | Testo 605i | Relative humidity (%) | 0-100%RH | ±3%RH (10%-35%RH)<br>±2%RH (35%-65%RH)<br>±3%RH (65%-90%RH)<br>±5%RH (<10% or >90%RH) |
| Thermo-Anemometer | Testo 405i | Flow velocity | 0-30m/s | ±0.1m/s (0-2m/s)<br>±0.3m/s (2-15m/s) |

For this initial stage, we are most concerned about the inlet temperature and humidity of the m-cycle experimental device, the temperature of the supply air, and the temperature and humidity of the working air. Therefore, three main points of inlet and outlet have been set to obtain the data of current humidity ratio and temperature, as

shown in Fig.3.2. In addition, ducts were set up at the outlet of the supply air and the outlet of the working air to reduce the impact of the export effect on the results.
After comparing the experimental inlet and outlet data with the simulation results, conclusions can be drawn on the accuracy of the simulation model.

## 3.2 Model validation using the experimental result

### 3.2.1 Environmental parameters:

The experiment was carried out in an environmental chamber, Kyushu University. Which carried out at the controlled inlet air conditions of 35%-45%RH, 25-35℃, as shown in Fig.3.9.

a


b

Fig.3.9 (a) Control panel; (b) Environmental chamber

### 3.2.2 Control parameter

By adjusting the setting parameter (temperature and relative humidity) of the environmental chamber, we can cover most summer conditions, when people need to run refrigeration equipment. Changing the input voltage of the power supply can change the speed of the fan; we can also manually adjust the working ratio by adjusting the opening degree of the grille. Therefore, four variables: inlet temperature, inlet humidity, inlet air velocity and working ratio were chosen as test variables in this experiment. Computer simulation was carried out under the identical working conditions as the above experimental setting, the specific results are as follows:

1) Inlet temperature:

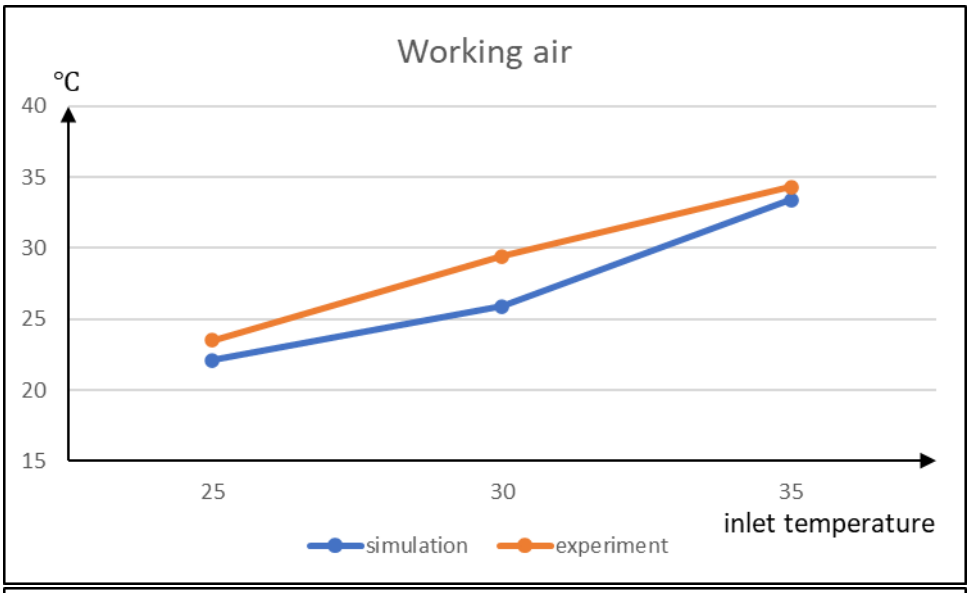


a

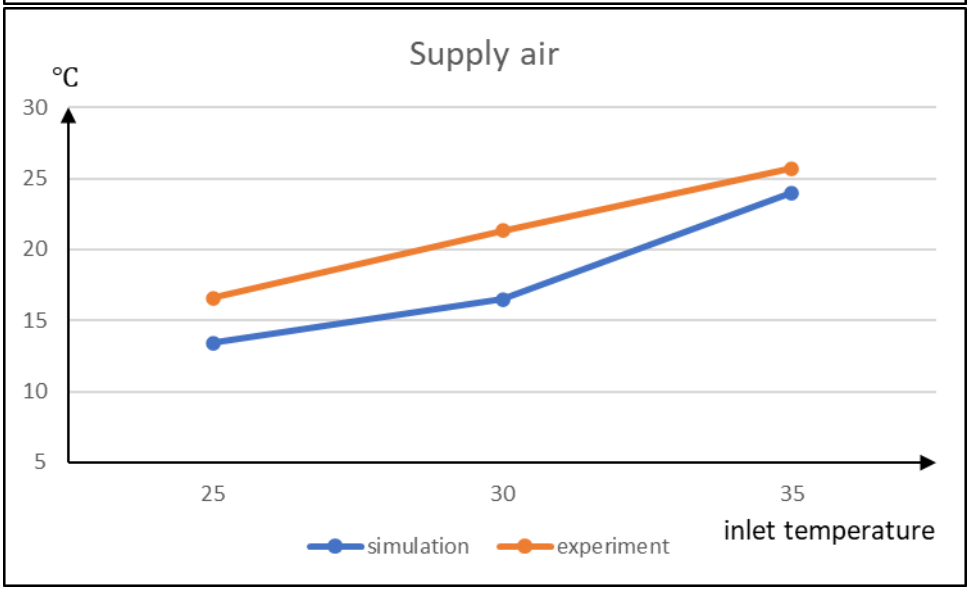


b

c

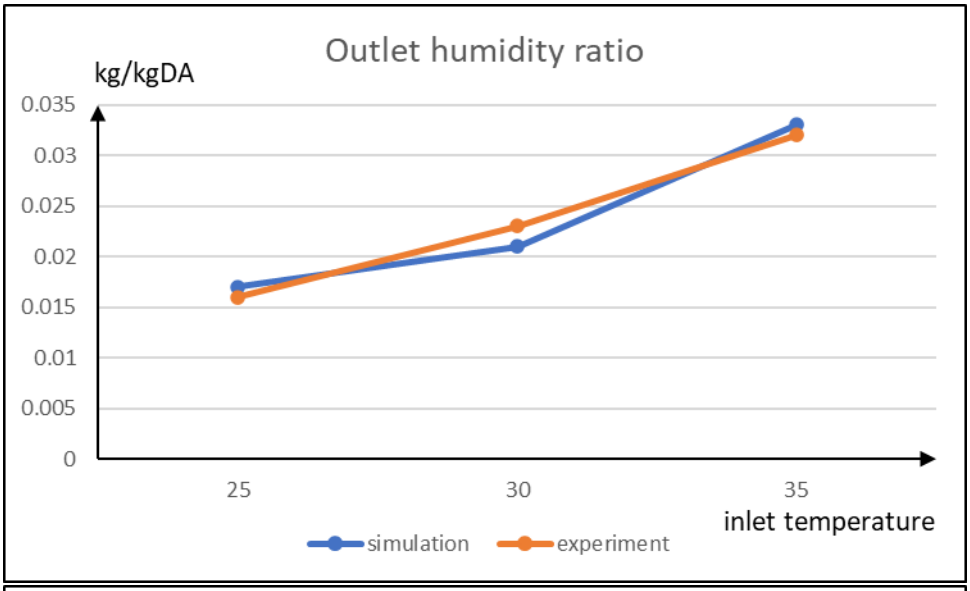


d

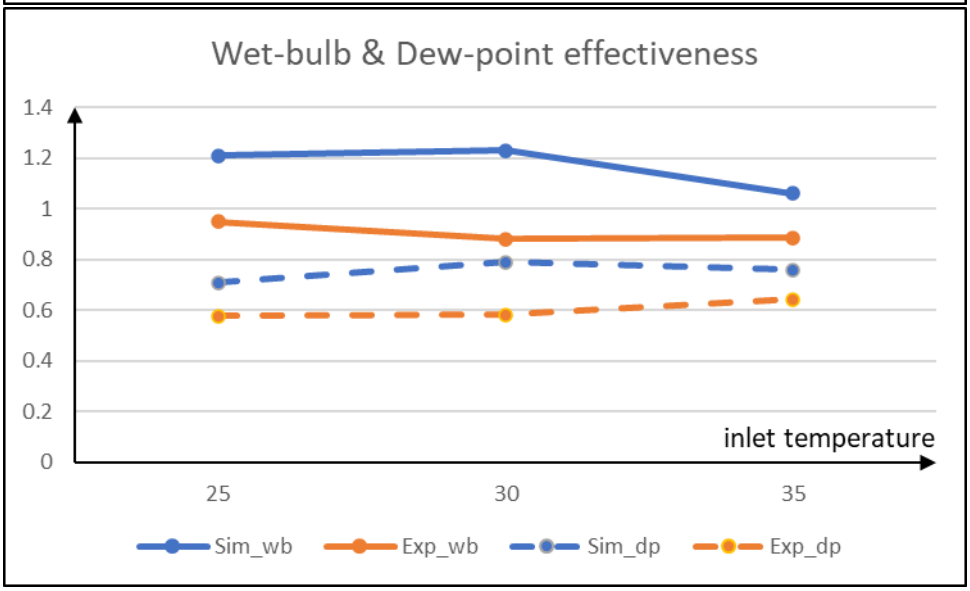


e

| ERROR | working | supply | humidity | wbE | dpE |
|---|---|---|---|---|---|
| 25 | 0.063 | 0.239 | 0.059 | 0.217 | 0.189 |
| 30 | 0.135 | 0.291 | 0.095 | 0.284 | 0.263 |
| 35 | 0.027 | 0.071 | 0.030 | 0.164 | 0.155 |

Fig.3.10 Comparison of experimental and simulation results with different inlet air temperature. (a)working air; (b)supply air; (c)outlet humidity ratio; (d)wet bulb and dew point effectiveness; (e)error between experimental and simulation value.

According to the Fig.3.10 shown above, the curve trends of the experimental data and the simulation data under this working condition are roughly the same, and the results of the two are relatively close, and the average error between the data is 15.2%. There is a large error between the experimental and simulation data under the working condition of 30℃.

2) Inlet humidity ratio:

a

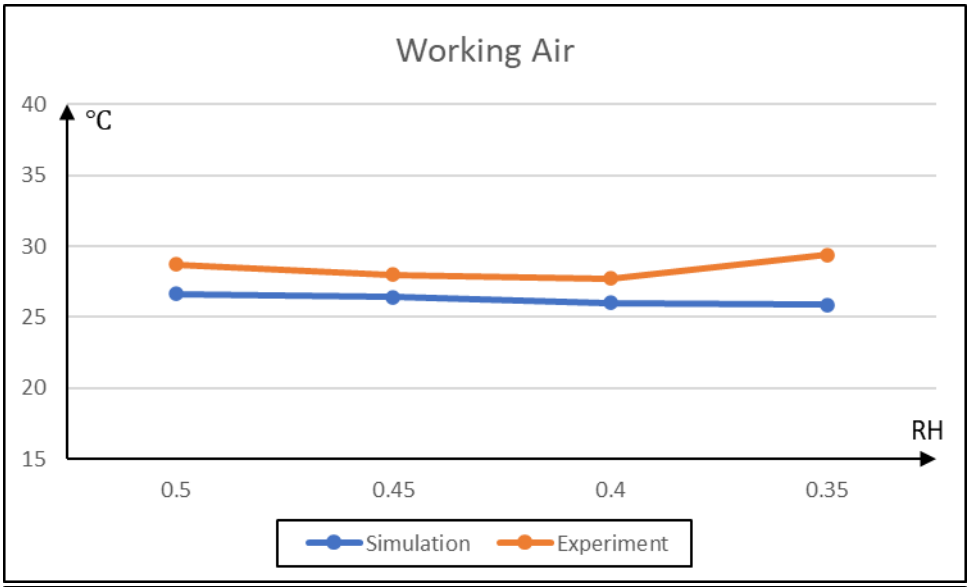


b

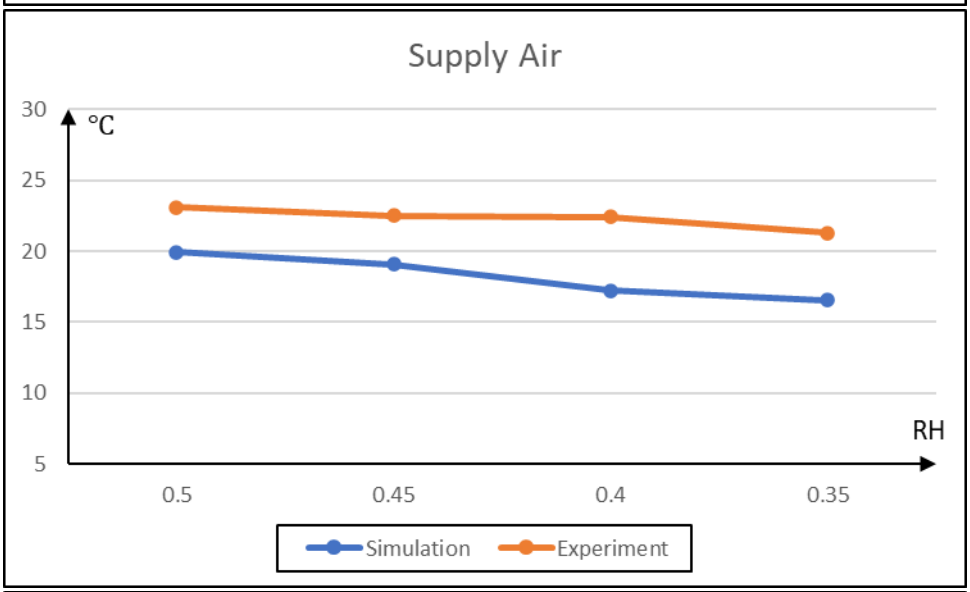


c

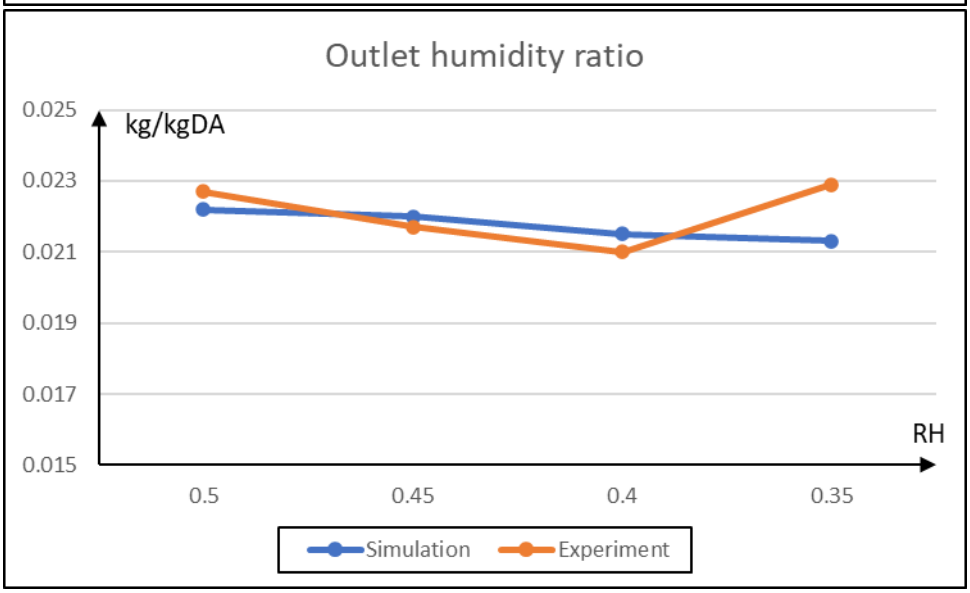

d

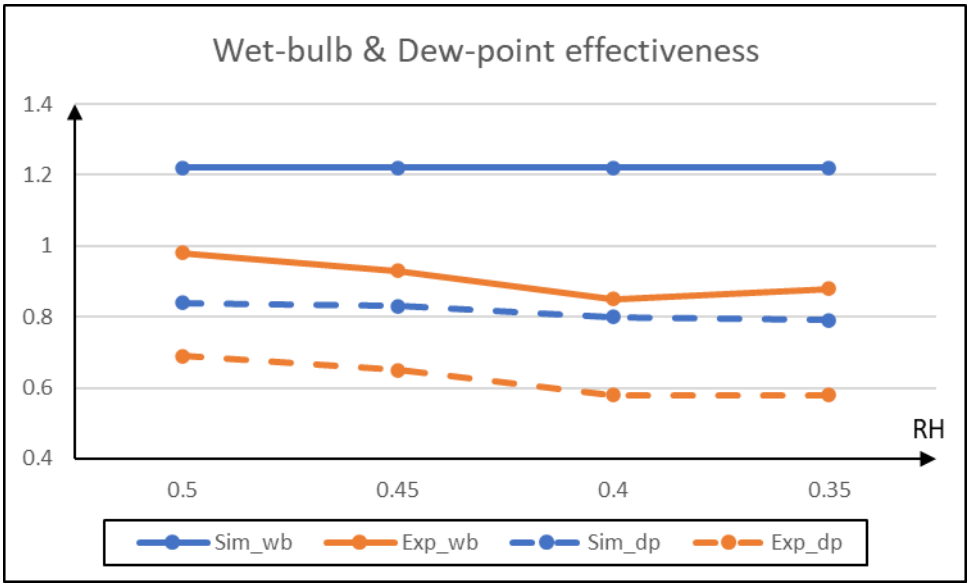


e

| ERROR | working | supply | humidity | wbE | dpE |
|---|---|---|---|---|---|
| 0.5 | 0.077 | 0.159 | 0.023 | 0.197 | 0.179 |
| 0.45 | 0.059 | 0.180 | 0.014 | 0.238 | 0.217 |
| 0.4 | 0.065 | 0.300 | 0.023 | 0.303 | 0.275 |
| 0.35 | 0.136 | 0.286 | 0.075 | 0.279 | 0.266 |

Fig.3.11 Comparison of experimental and simulation results with different inlet RH. (a)working air; (b)supply air; (c)outlet humidity ratio; (d)wet bulb and dew point effectiveness; (e)error between experimental and simulation value.

By changing the inlet air humidity ratio, the variation trend of the experimental results and the simulation results is roughly the same. However, when the RH is equal to 35% and 40%, the data is quite different from the simulation results, which is reflected in the temperature of the outlet supply air. Considering that the actual experimental temperature is higher than the simulation results, the outlet humidity is lower than the simulation results. There is insufficient humidity in the wick material in the wet channel during the test. The average error under this condition is 16.7%.

3) Inlet air velocity:

a

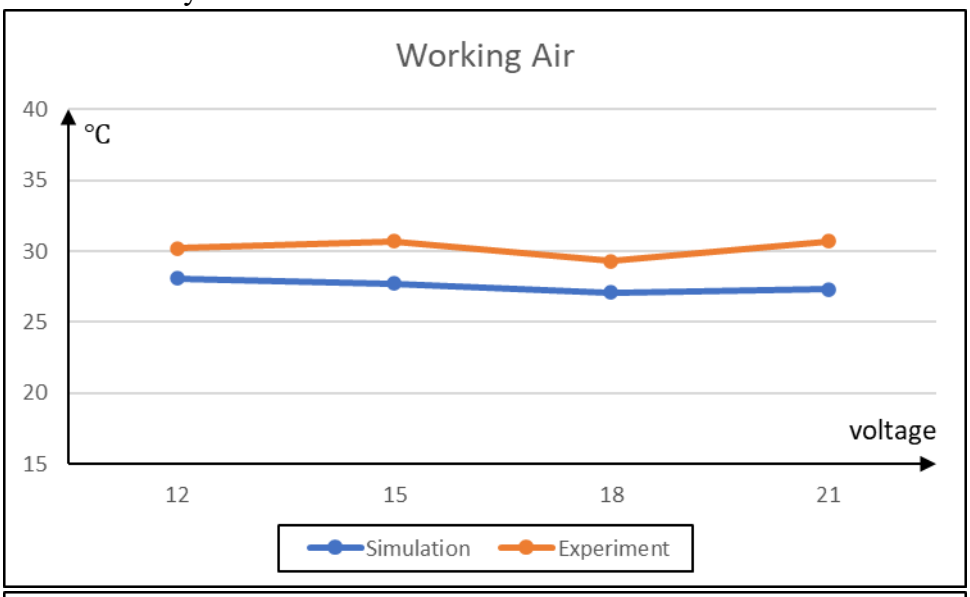


b

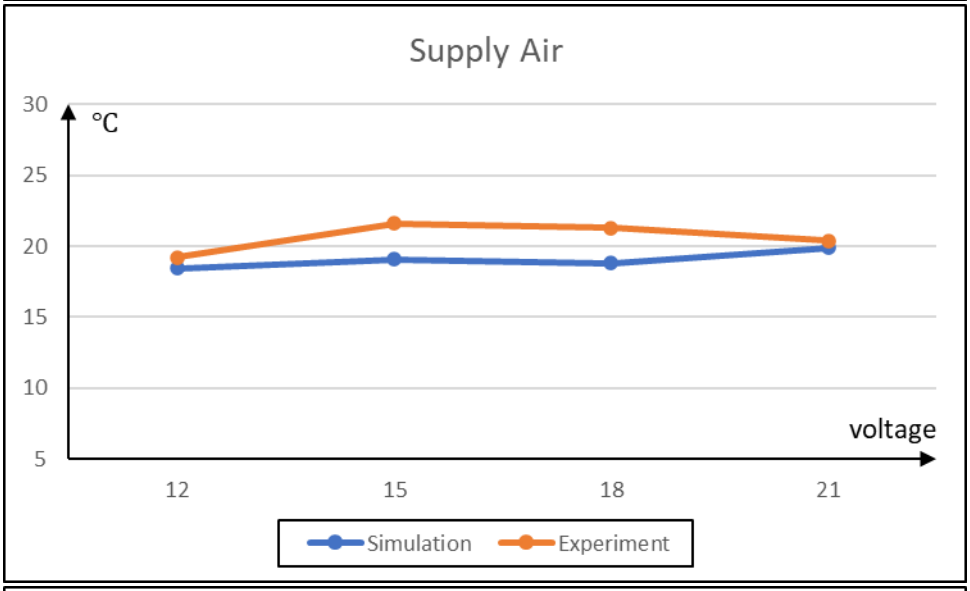


c

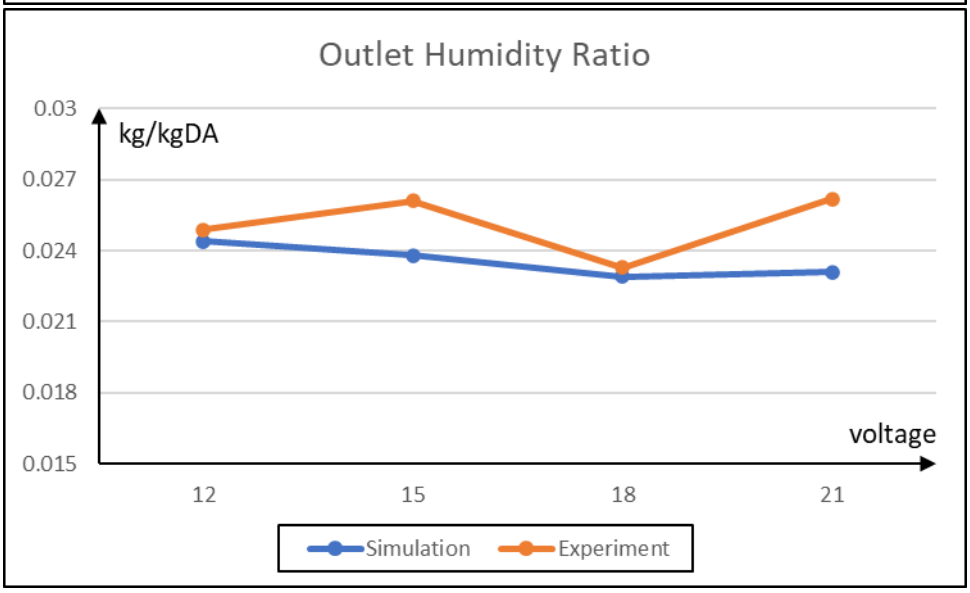

d

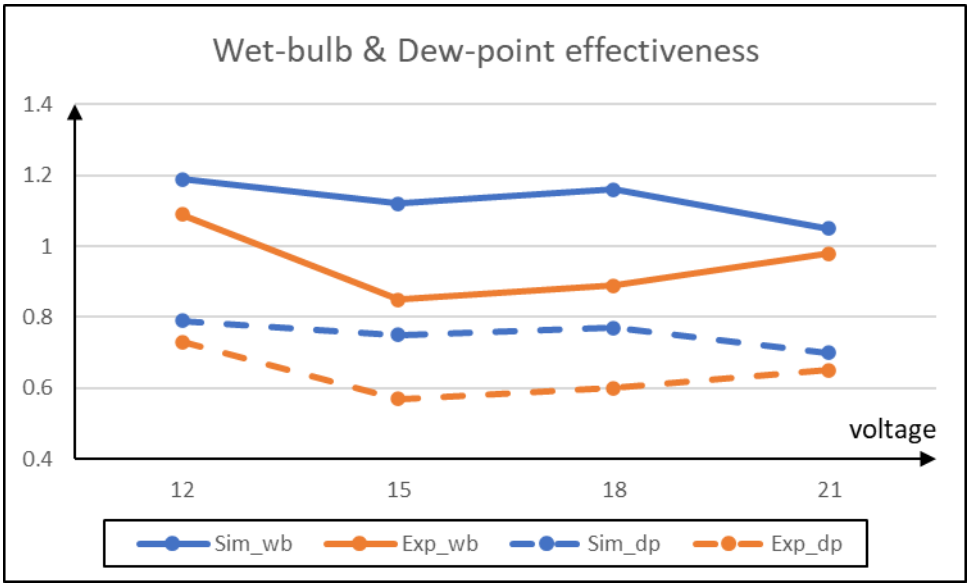


e

| ERROR | working | supply | humidity | wbE | dpE |
|---|---|---|---|---|---|
| 12 | 0.075 | 0.041 | 0.020 | 0.084 | 0.076 |
| 15 | 0.108 | 0.133 | 0.097 | 0.241 | 0.240 |
| 18 | 0.081 | 0.133 | 0.017 | 0.233 | 0.221 |
| 21 | 0.125 | 0.025 | 0.134 | 0.067 | 0.071 |

Fig.3.12 Comparison of experimental and simulation results with different inlet velocity. (a)working air; (b)supply air; (c)outlet humidity ratio; (d)wet bulb and dew point effectiveness; (e)error between experimental and simulation value.

The experimental results are not ideal under the condition of changing velocity, because the inlet air velocity is one of the important parameters affecting the performance of the system. The overall variation trend of the experimental results does not meet the expectations of the simulation results, but it is relatively close in terms of numerical values, with an average error value of 11.1%. The difference between the experimental data and the simulation results also shows that there are obvious air leakage and pressure drop in the actual experimental device.

4) Working ratio:

a

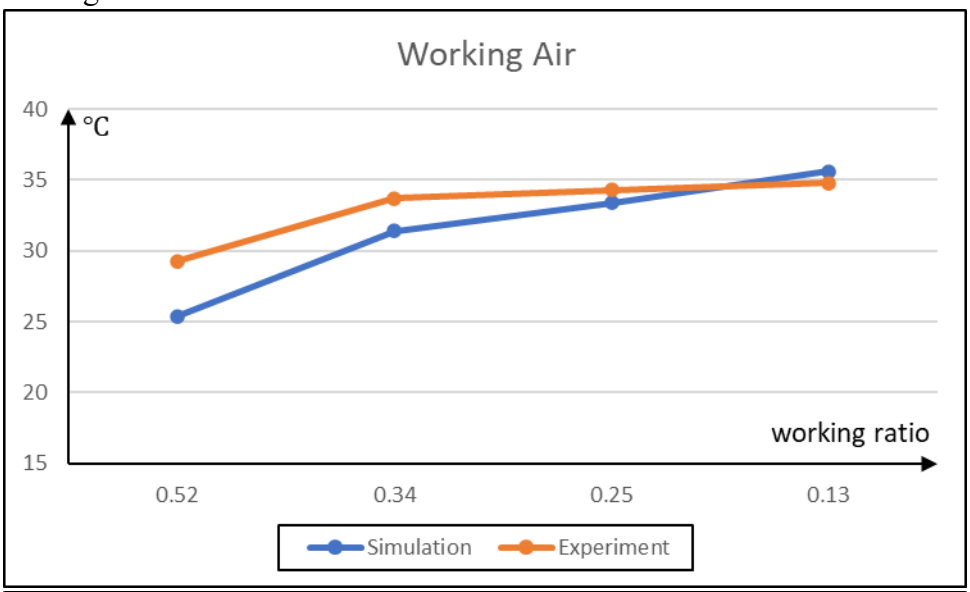


b

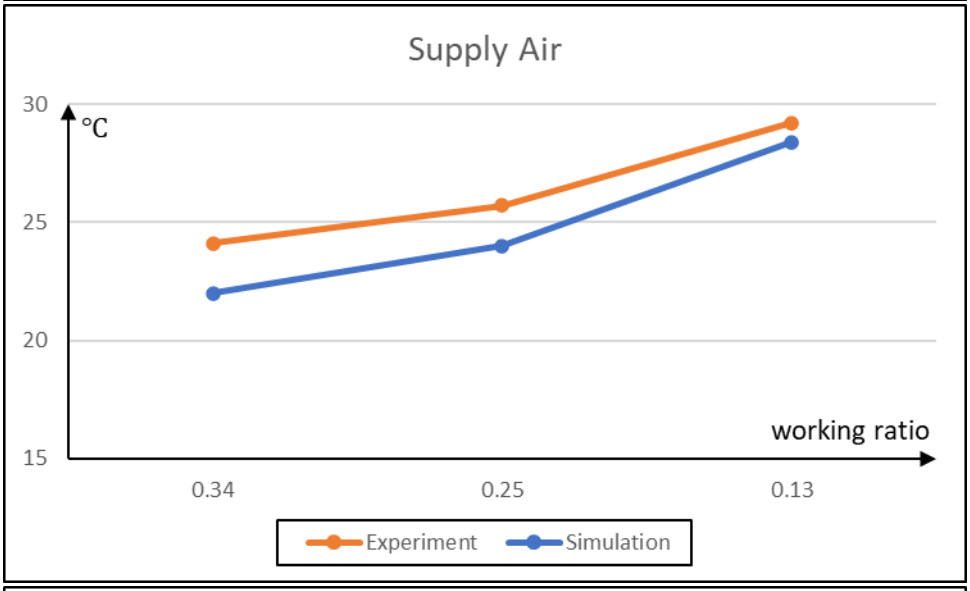


c

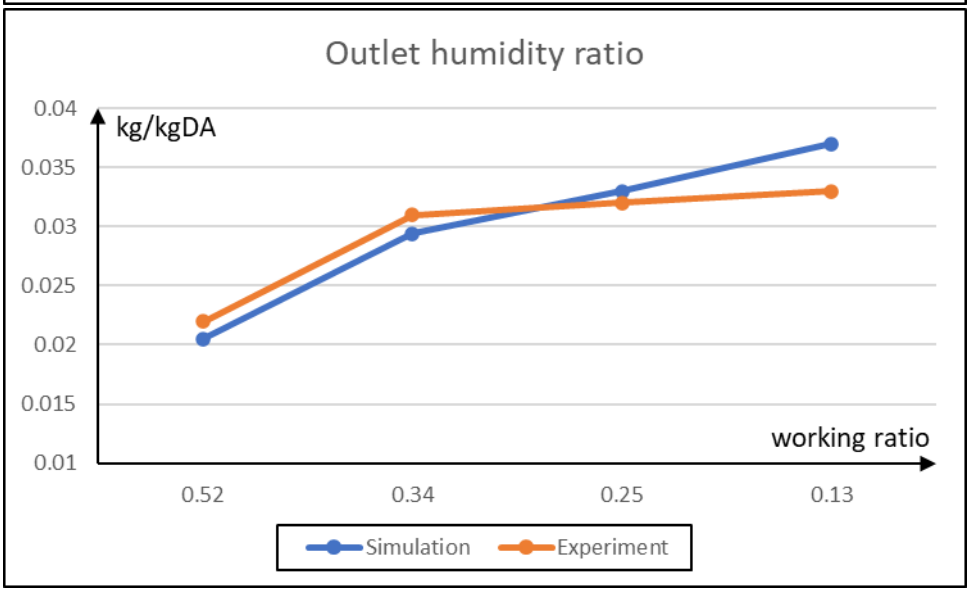

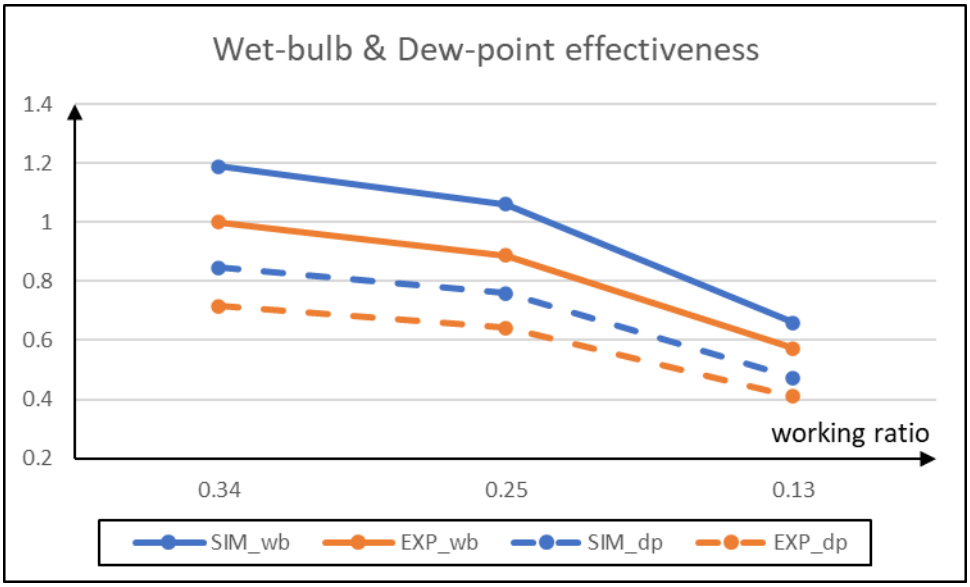


d

| ERROR | working | supply | humidity | wbE | dpE |
|---|---|---|---|---|---|
| 0.52 | 0.154 | | 0.073 | | |
| 0.34 | 0.073 | 0.095 | 0.054 | 0.159 | 0.151 |
| 0.25 | 0.027 | 0.071 | 0.030 | 0.164 | 0.155 |
| 0.13 | 0.022 | 0.028 | 0.108 | 0.131 | 0.131 |

e

Fig.3.13 Comparison of experimental and simulation results with different working ratio. (a)working air; (b)supply air; (c)outlet humidity ratio; (d)wet bulb and dew point effectiveness; (e)error between experimental and simulation value.

The experimental results obtained by changing the working ratio are the closest to the simulation results. It has an average error value of 9.3%. This is due to the fact that under this working condition, there is no need to change the temperature and humidity settings of the environmental chamber, which can ensure that the inlet air parameters remain in a stable state, and it is relatively simple to change the working ratio.

## 3.3 Discussion and summery

In practice, compared with the ideal conditions of the simulation model, there are unavoidable heat loss and air leakage in the actual experiment; the pressure drop in the channel is also larger than the value considered in the simulation model, which leads to the velocity loss of the working air. However, most of the error value between the experimental data and the simulation results is around 15%, which is an acceptable result. Therefore, based on the above analysis of the results, this simulation model can be considered to be able to better simulate the heat and mass transfer processes in the channel and to evaluate the performance of the system.

For the current prototype experimental setup, the shorter channel length may alleviate the pressure drop problem in the channel. A better wick material can better simulate the water film in the simulation model, and the continuous slow water supply also has a significant impact on the accuracy of the experimental results. On the other hand, from the simulation level, the introduction of test influence factors can also be helpful to simulate the inevitable air leakage and pressure drop in actual working conditions. Based on the above assumptions, the difference between the experimental results and the simulation results will be narrowed.

# Chapter 4 Result and discussion

In the previous chapter we have verified the simulation model. In this chapter, the results of the simulation model will be elaborated and the effects of different geometrical parameters, operational parameters on the temperature distribution, humidity distribution and performance in the channel will be analyzed.

## 4.1 Temperature and humidity distribution along the channels

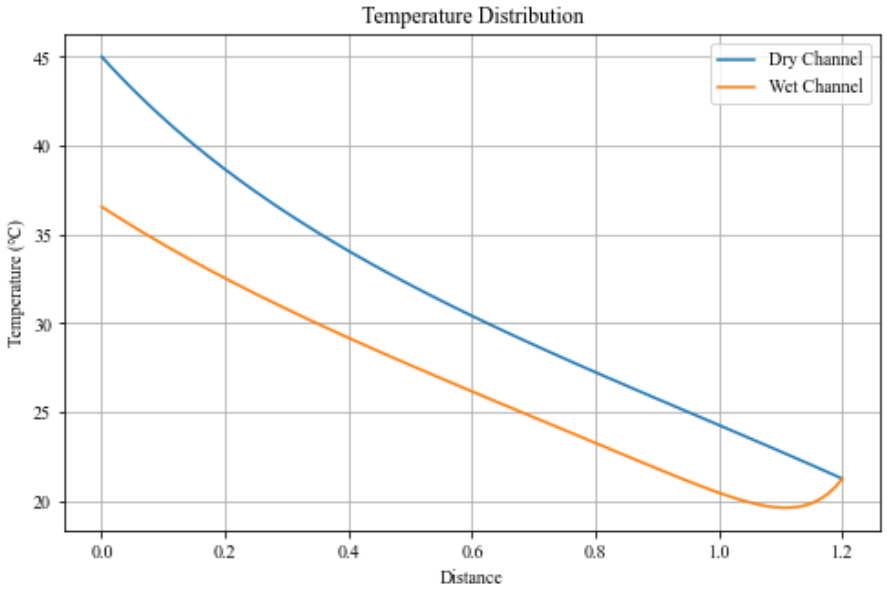


(a)

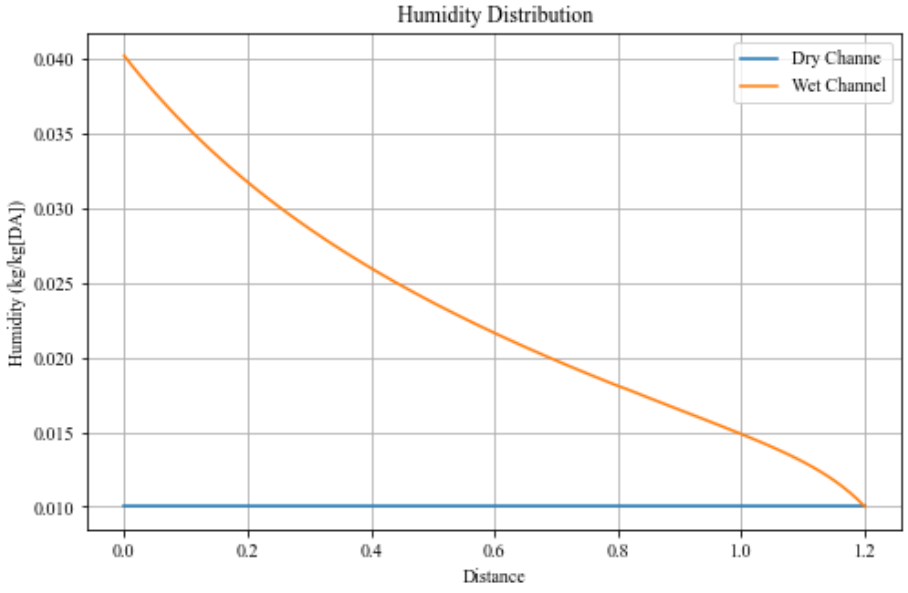


(b)

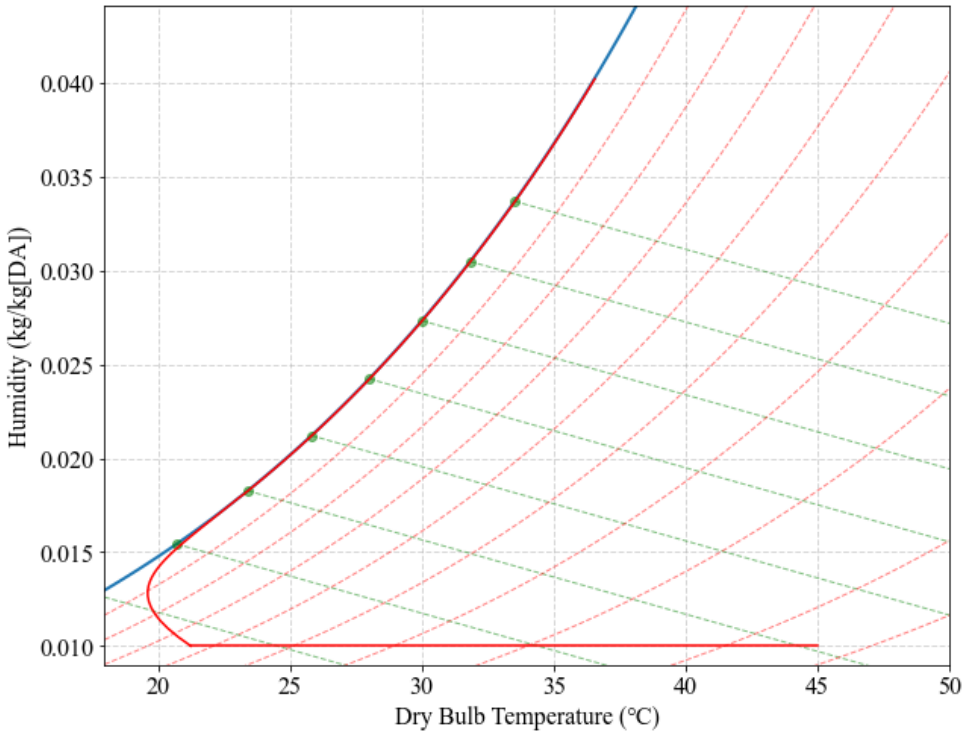


(c)

Fig.4.1 Temperature and humidity profiles. (a) Temperature distribution; (b) Humidity distribution; (c) Psychrometric chart.

Fig.4.1 (a) and (b) depict the temperature and humidity distribution of dry and wet channel with the inlet conditions: 45℃ inlet air temperature, 10g/kg inlet humidity ratio and 1.2m/s inlet air velocity with 0.3 working ratio. For the temperature distribution graph, air temperature along the dry channel is decreasing owing to the continuous convective heat transfer occurs inside the channel. When a part of the intake air enters the wet channel and becomes the working air, the air temperature decreases first. This is because the air temperature at this time is higher than the water film temperature, and the sensible heat is transferred from the working air to the water film. When the air temperature is consistent with the water film temperature is the minimum temperature of the working air. After that, the temperature of the working air continued to increase, which is because the evaporation process of the water film continued to obtain heat from the dry channel, so that the temperature of the water film was higher than that of the working air, and the heat was transferred from the water film to the working air.

For the humidity distribution graph, combined with Fig.4.1 (c), the humidity of the intake air remains constant. The working air continues to increase after entering the wet channel, and the working air soon reaches saturation. However, although the air is saturated, the humidity ratio continues to rise, as the water layer continues to gain heat from the dry channels, which has caused the evaporation process to continue. In this showing case, the working air became saturated when the humidity ratio is over 15g/kg, at approximately 0.4 meters from the entrance to the wet channel, and the outlet

humidity ratio of the working air is around 40g/kg.
According to the saturation position, the graphs below show how different conditions affect it:

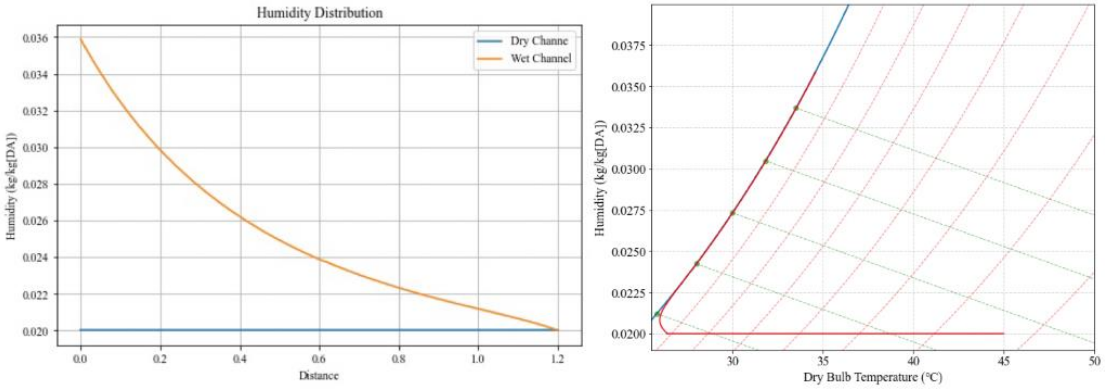


(a) inlet humidity ratio 20g/kg.

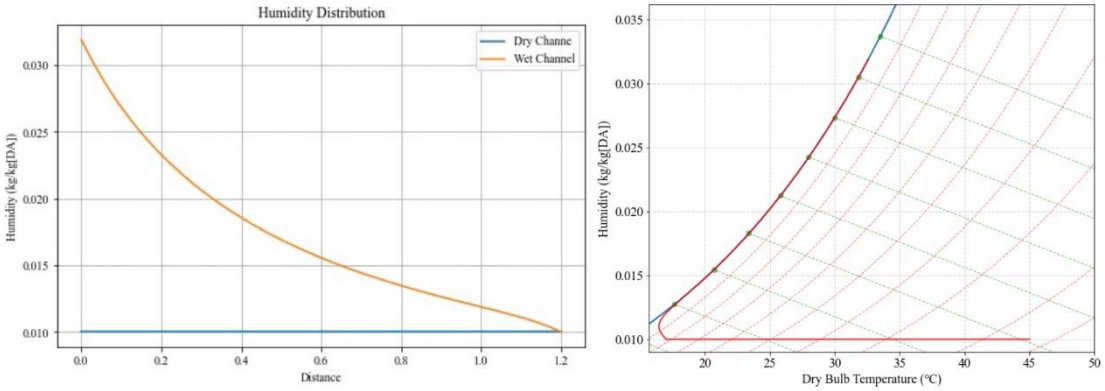


(b) inlet air velocity 1.0m/s.

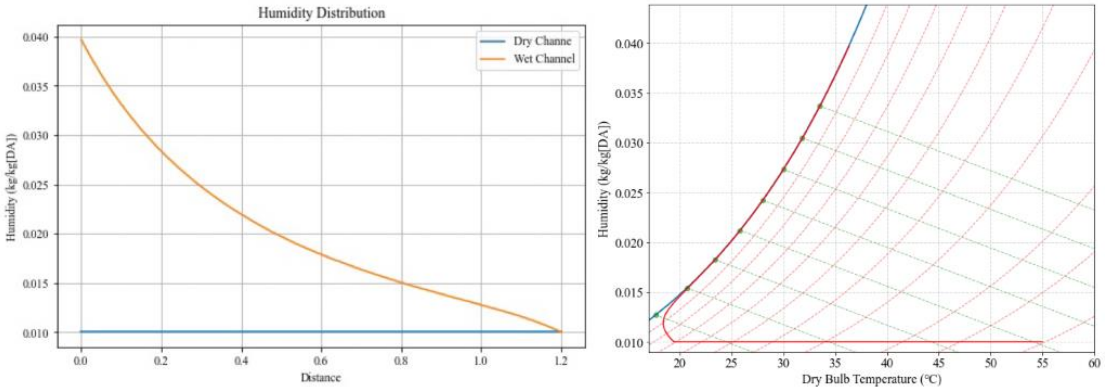


(c) inlet air temperature 55℃.

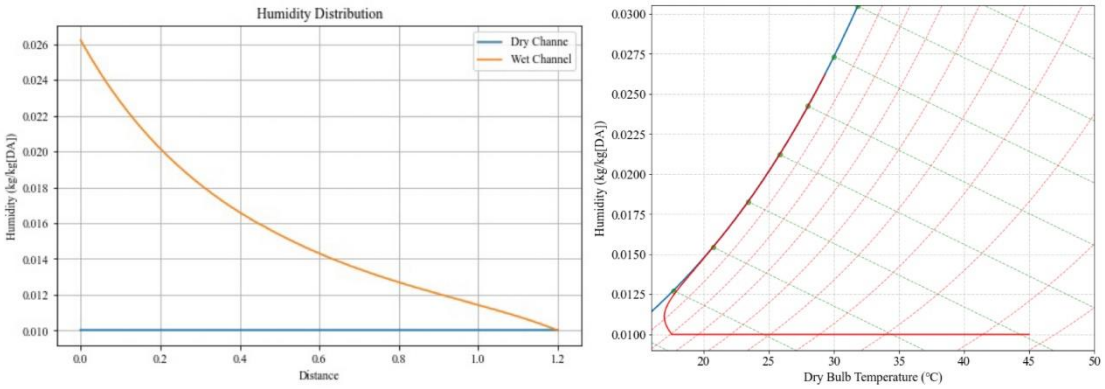


(d) working ratio 0.7.

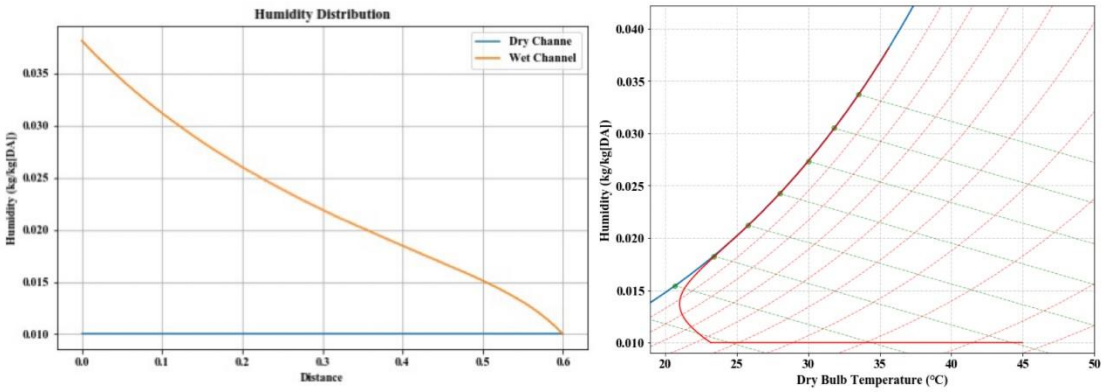


(e) channel length 0.6m.

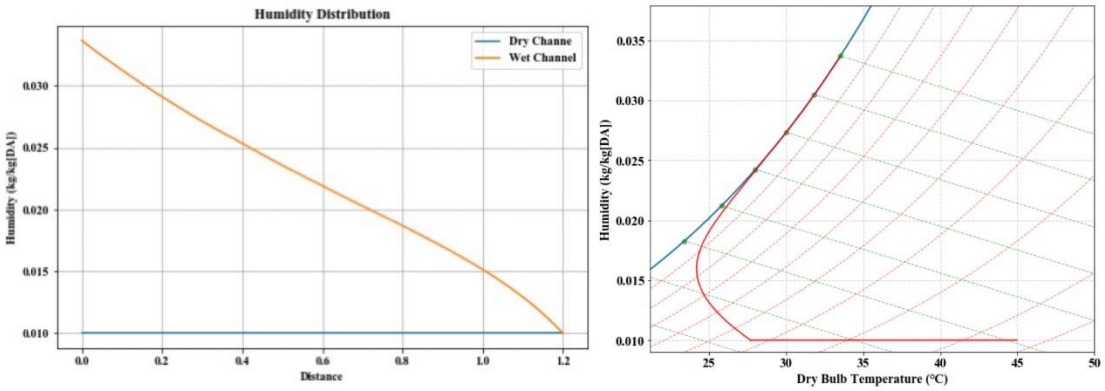


(f) channel height 0.009m.

Fig.4.2 The influence of different parameters on the air saturation point.

Comparing the above figures with the previous working conditions (Fig.4.2), we can know that: Inlet parameters such as temperature, velocity and humidity have little effect on the position of the air saturation point; in terms of geometric structure, the length of the channel also has little effect on the position of the saturation point. Among the above test parameters, working ratio and channel height have obvious influence on the position. More unsaturated air entering the wet channel means that more water needs to be absorbed to reach saturation. Under the condition of the same amount of heat

obtained from the dry channel, the time required for the air to reach saturation in the wet channel becomes longer, that is to say, the location of the saturation point becomes farther from the entrance of the wet channel.

## 4.2 The impact of changing different parameters on performance

In practical engineering applications, devices often cannot operate under ideal conditions. Therefore, analyzing the impact of environmental factors on device performance is crucial for the pursuit of higher efficiency, energy conservation, and environmentally friendly. The factors that affect the performance of the system can be roughly divided into two types: air inlet parameters and system geometry parameters. The following section analyzes the influence of these parameters on the heat transfer performance of the system by changing the inlet air temperature, humidity ratio, velocity, working ratio, channel length and channel height.
The basic specifications of the parameters used in this simulation is given below:

Table 4.1: Basic specifications of the parameters used in simulation.

| Parameters | Specification/Values |
|---|---|
| Air inlet temperature (℃) | 25 |
| humidity ratio (kg/kgDA) | 0.01 |
| Wall thickness(mm) | 0.45 |
| Channel length(m) | 1.0 |
| Channel width(mm) | 83 |
| Channel height(mm) | 4.5 |
| Working ratio (-) | 0.5 |
| Air inlet velocity (m/s) | 1.4 |

### 4.2.1 Inlet air temperature

The inlet air temperature varies from 25℃ to 45℃ while the inlet humidity ratio and others parameters remain unchanged.

a

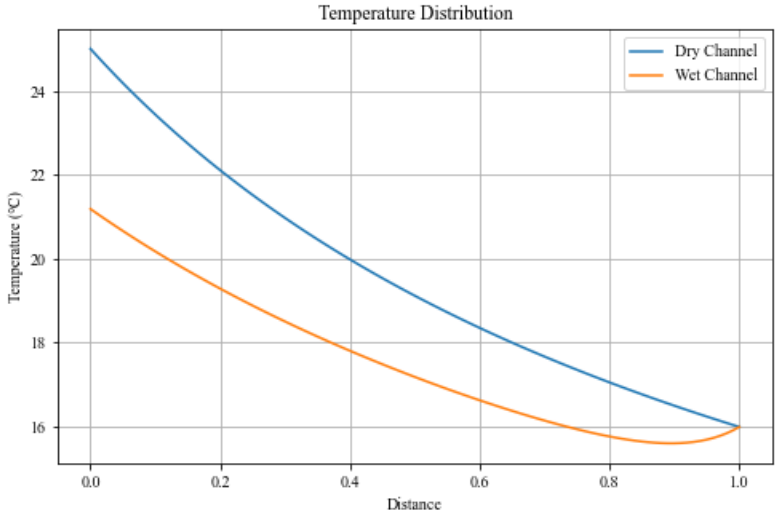


b

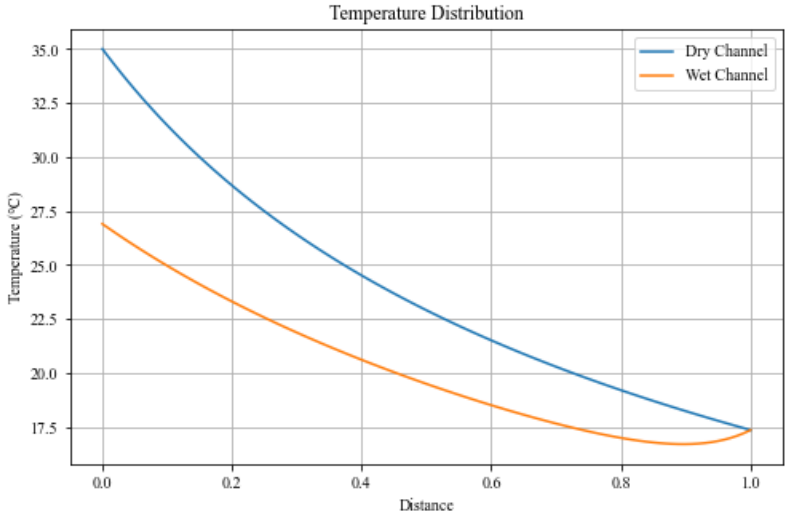


c

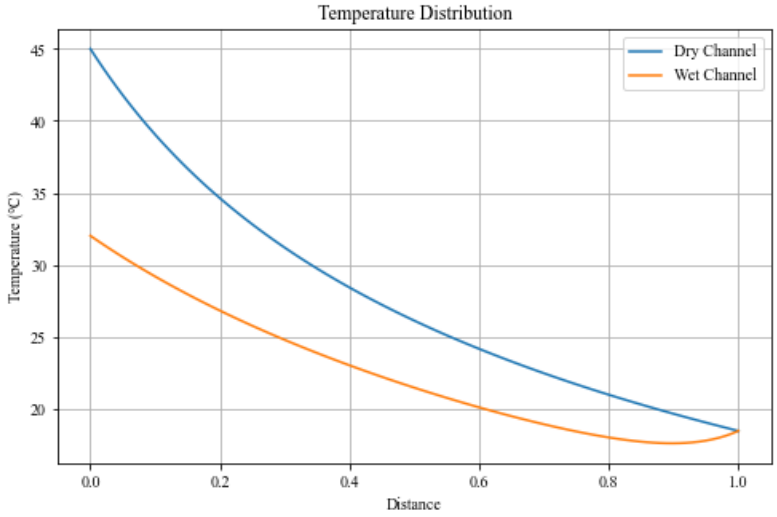

Fig.4.3 Temperature distribution of different inlet T: (a) 25℃; (b) 35℃; (c) 45℃.

a

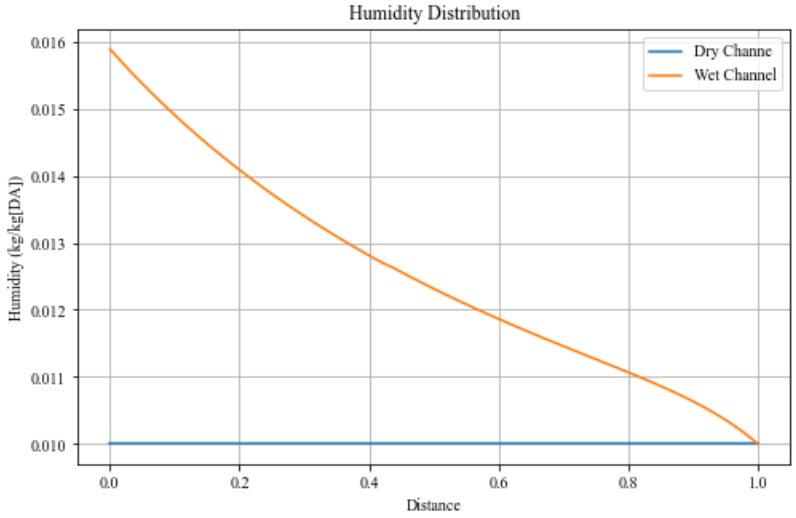


b

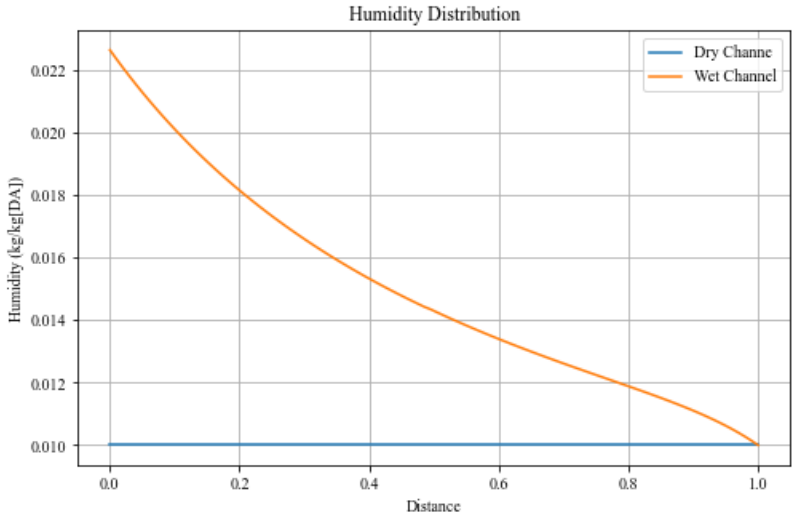


c

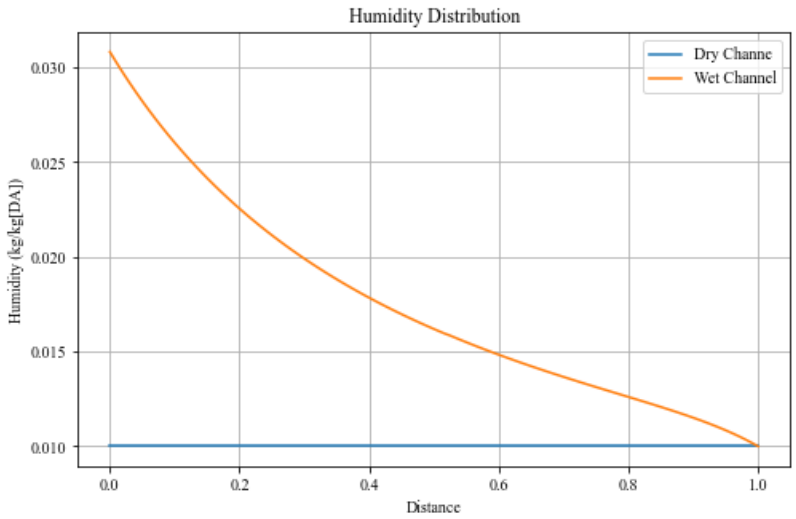


Fig.4.4 Humidity distribution of different inlet T: (a) 25℃; (b) 35℃; (c) 45℃.

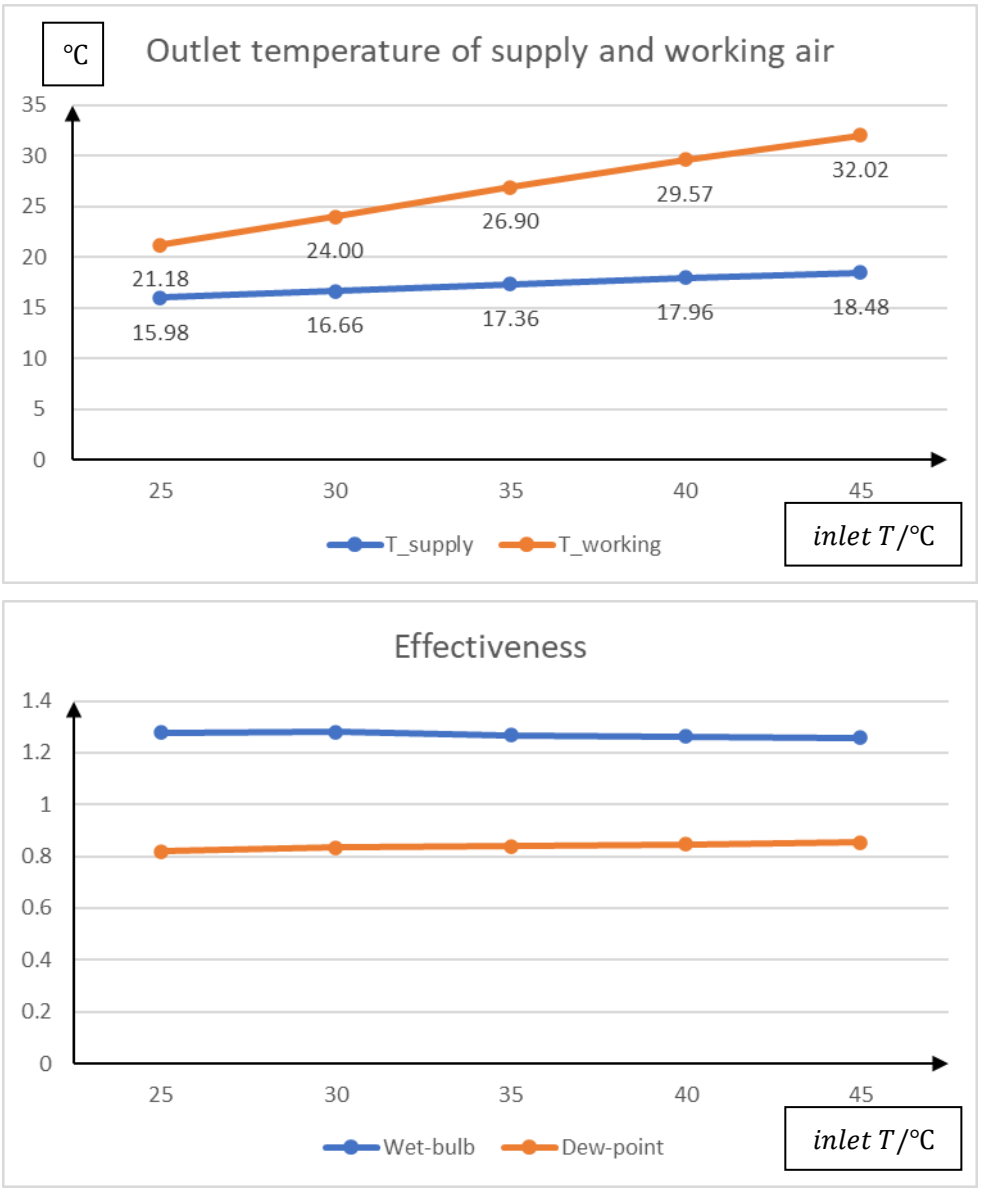


Fig.4.5 Comparison of output parameters at different inlet temperatures

The above image shows that the inlet air temperature has little effect on the trend of the temperature and humidity distribution curves in the channel. The outlet temperature and humidity of the working air and the outlet temperature of the supply air all increase with the increase of the inlet temperature, and the dew point efficiency also increases slightly, range from 0.81 to 0.85. However, it can also be seen from the figure that the change in inlet temperature has a negligible increase in wet bulb efficiency (the value of the wet-bulb effectiveness is around 1.27). The higher inlet temperature will make the evaporation process in the wet channel more intense, which can also be seen from the increase of the temperature and humidity of the working air.

### 4.2.2 Inlet air humidity ratio

The inlet air humidity ratio varies from 0.005 to 0.02kg/kgDA.

a

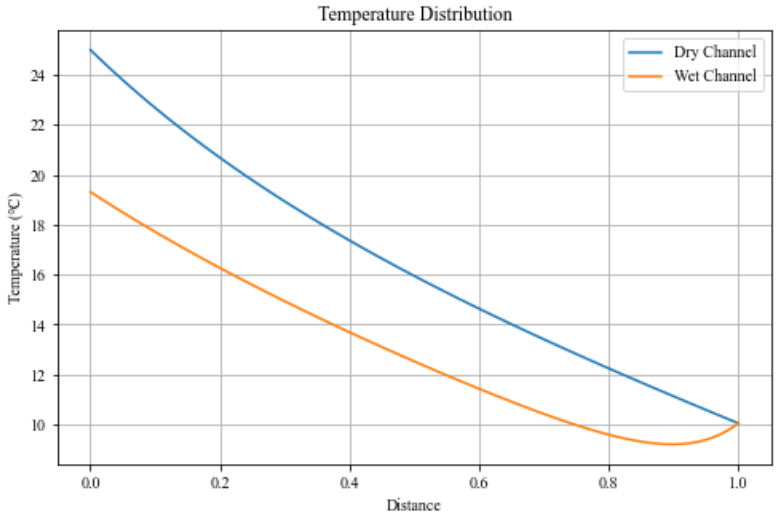


b

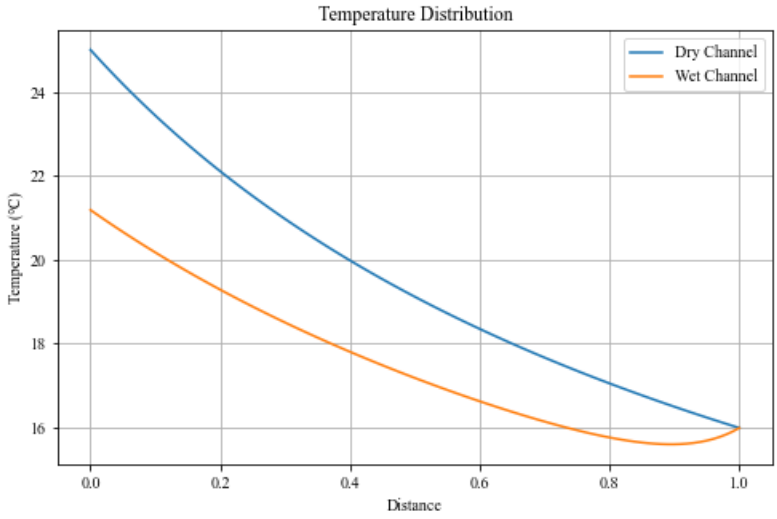


c

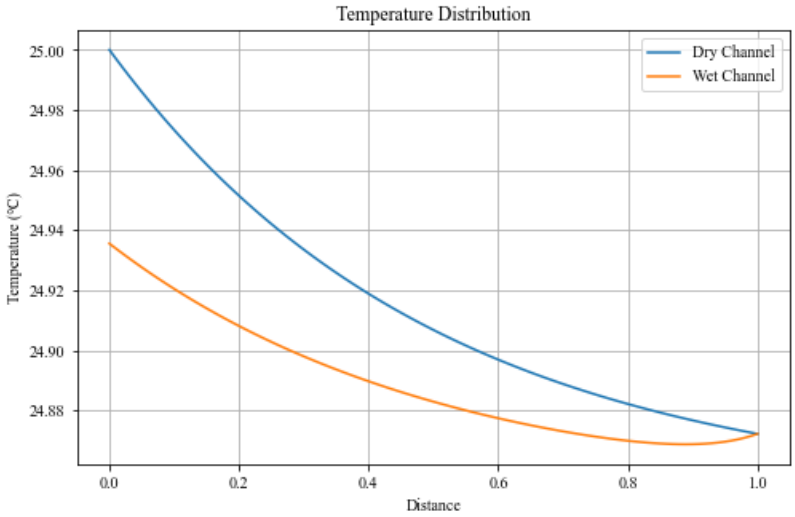


Fig.4.6 Temperature distribution of different inlet humidity ratio: (a) 0.005kg/kgDA; (b) 0.01kg/kgDA; (c) 0.02kg/kgDA.

a

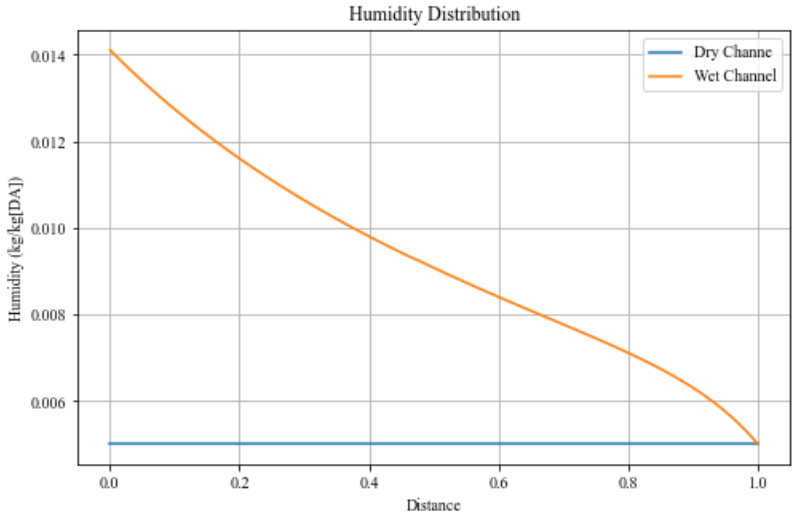


b

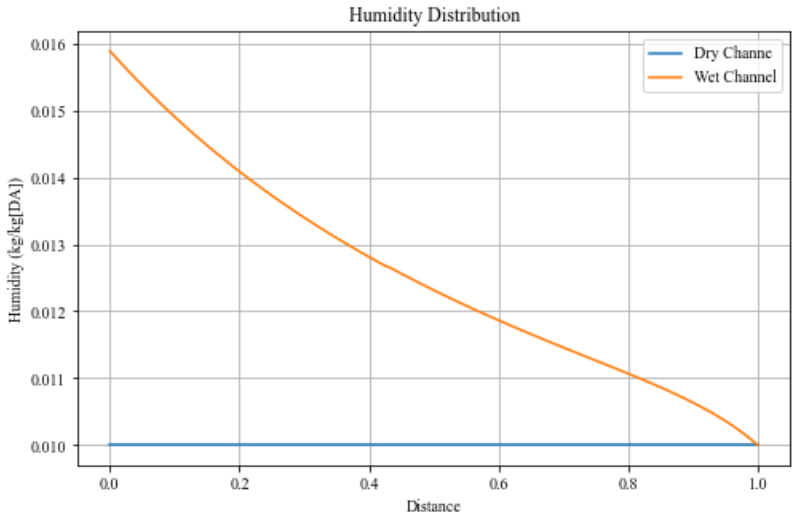


c

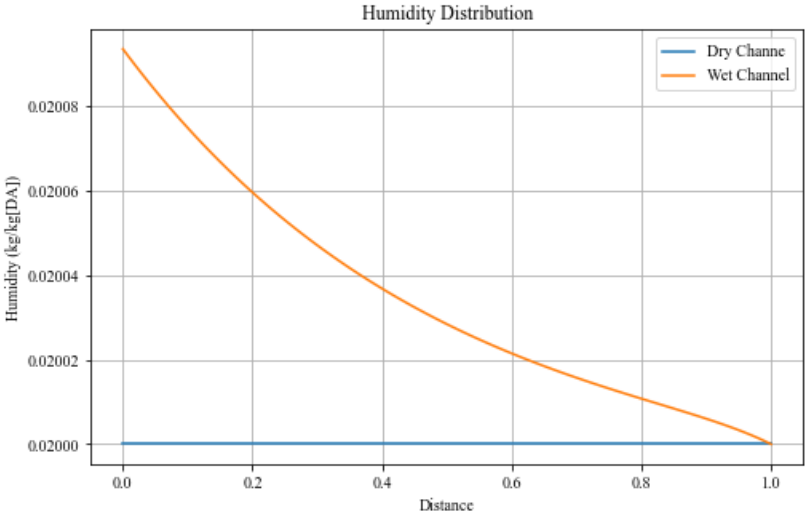


Fig.4.7 Humidity distribution of different inlet humidity ratio: (a) 0.005kg/kgDA; (b) 0.01kg/kgDA; (c) 0.02kg/kgDA.

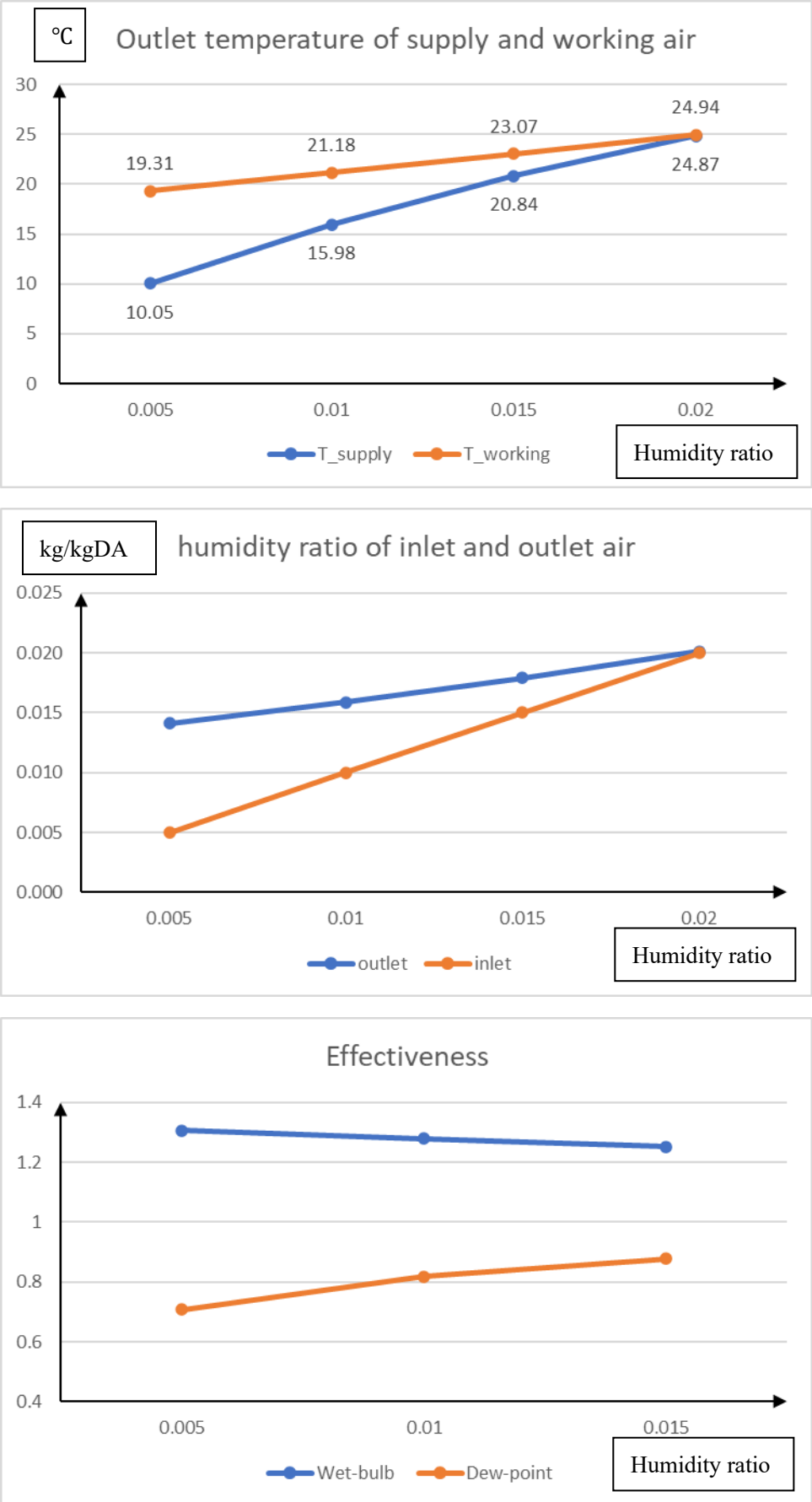


Fig.4.8 Comparison of output parameters at different inlet humidity ratio.

The above graph depicts that the inlet humidity also has little effect on the trend of the temperature and humidity curves in the channel. As the inlet humidity increases, the outlet temperature and humidity of the working air, the outlet temperature of the supply and the dew point efficiency (varies from 0.7 to 0.91) of the system will also increase. Just like the effect of inlet temperature on wet bulb efficiency, the effect of inlet humidity on it is also very small, only changing from 1.25 to 1.3. However, if the inlet air is close to saturation, as shown in the first and second pictures in Fig, the inlet air humidity is 0.02kg/kgDA in this working condition, and the concentration difference between the working air and the water film is very small, which means the evaporation process basically does not occur in the wet channel, therefore the temperature and humidity of the inlet and outlet of the working air are basically the same. This also proves that the dew point cooler can only perform well under low humidity conditions.

### 4.2.3 Inlet air velocity

The inlet air velocity varies from 1.0 to 3.0 m/s.

a

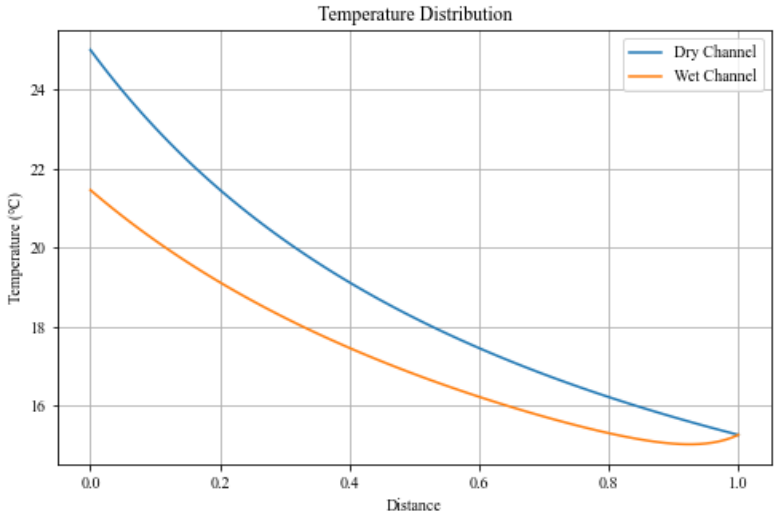


b

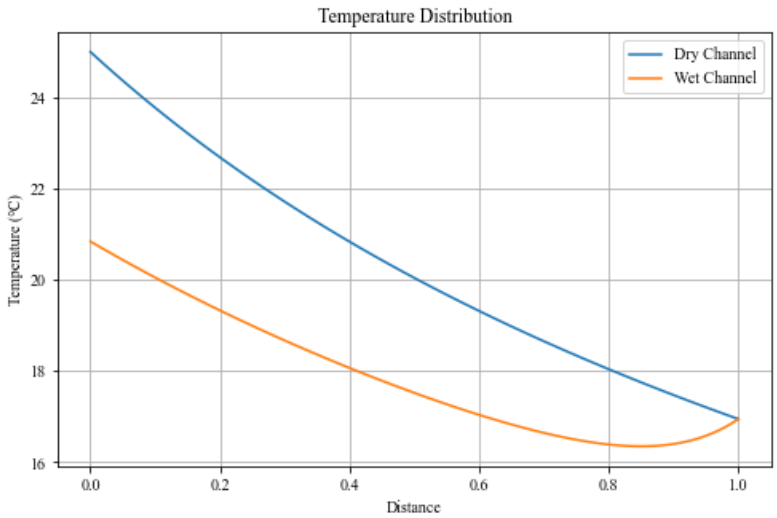


c

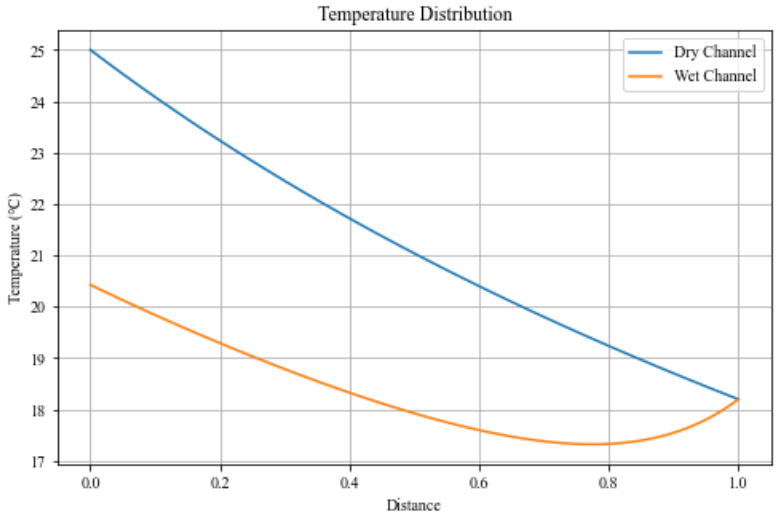


Fig.4.9 Temperature distribution of different inlet velocity: (a) 1.0 m/s; (b) 2.0 m/s; (c) 3.0 m/s.

a

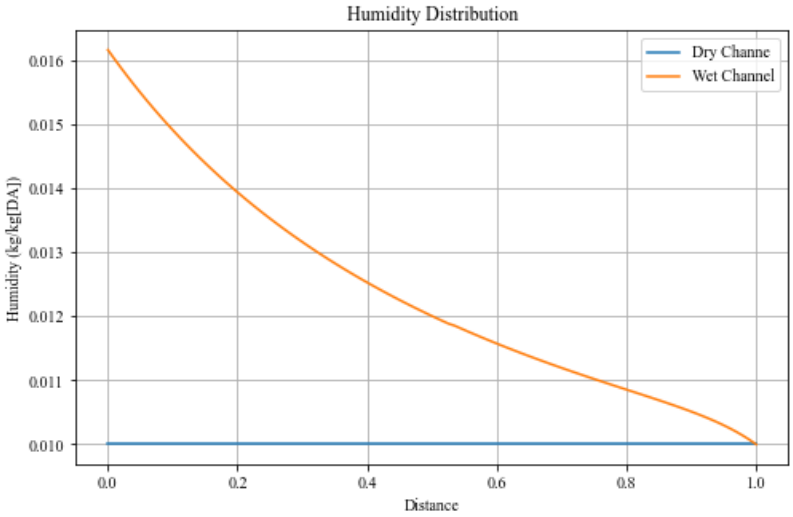


b

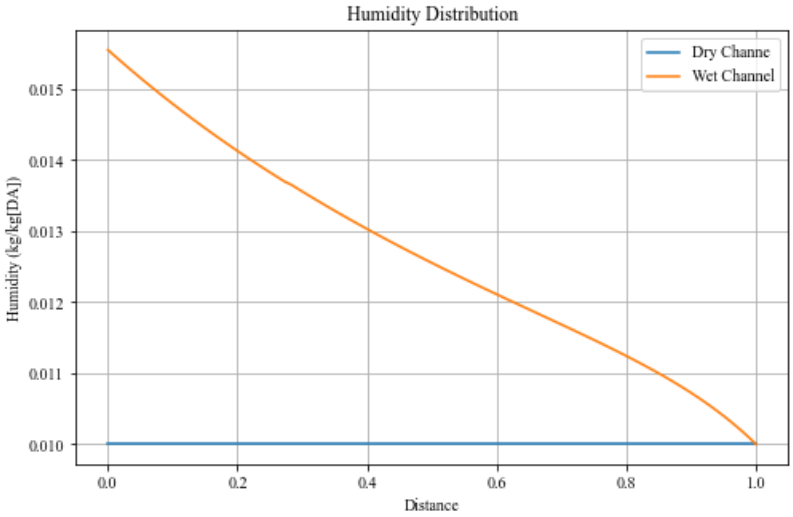


c

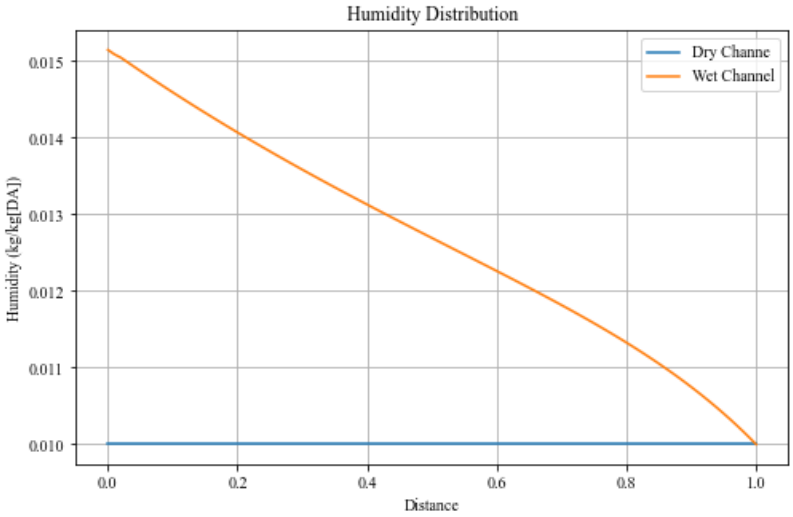


Fig.4.10 Humidity distribution of different inlet velocity: (a) 1.0 m/s; (b) 2.0 m/s; (c) 3.0 m/s.

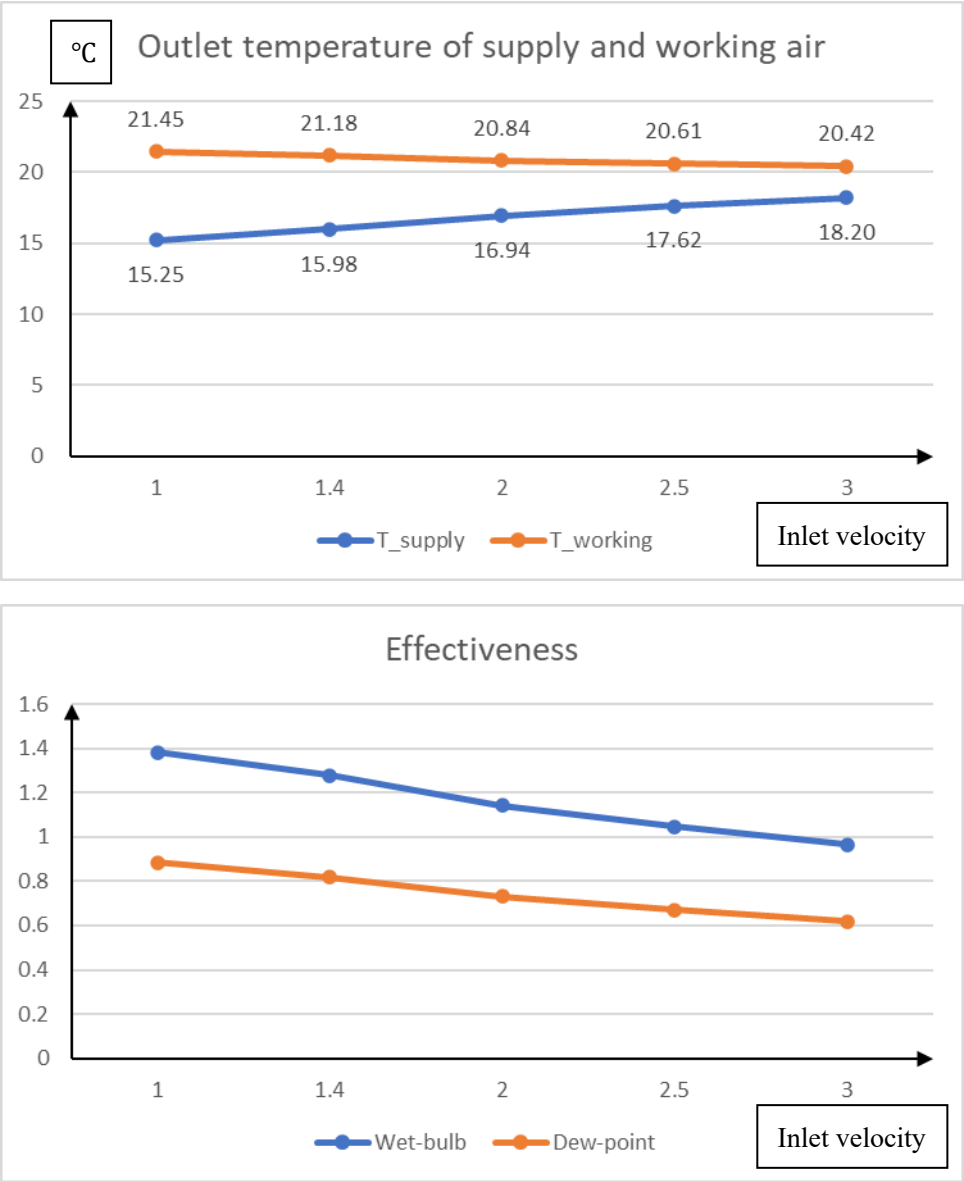


Fig.4.11 Comparison of output parameters at different inlet velocity.

Changing the speed of the inlet air will intuitively change the Reynolds number and Nusselt number of the airflow, and will affect the heat and mass transfer processes between the wet and dry channels and the water film. This can also be easily seen from the changes in the temperature and humidity distribution figures at different inlet velocities. What's more, the cooling capacity of the system is also closely related to the inlet air velocity, with the increase of the inlet velocity, the wet-bulb efficiency and the dew-point efficiency decrease, from 1.38 to 0.96 and 0.88 to 0.62, respectively. Due to this relatively weak heat and mass transfer process, the air in the dry channel loses less heat and the air in the wet channel gains less heat, resulting in an increase in the temperature of the supply air and a decrease in the temperature of the working air.

### 4.2.4 Working ratio

The working ratio varies from 0.3 to 1.0.

a

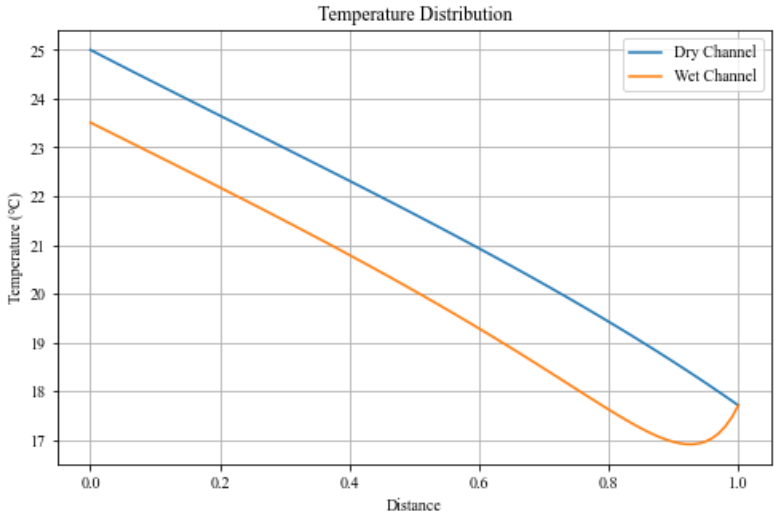


b

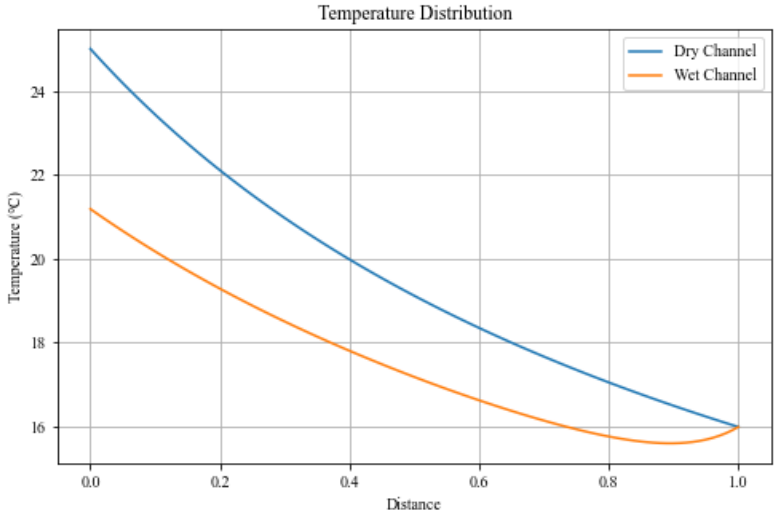


c

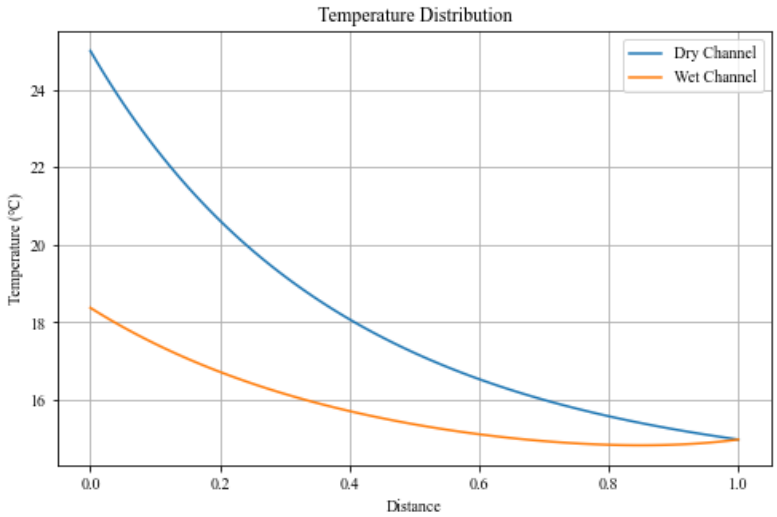


Fig.4.12 Temperature distribution of different working ratio: (a) 0.3; (b) 0.5; (c) 1.0.

a

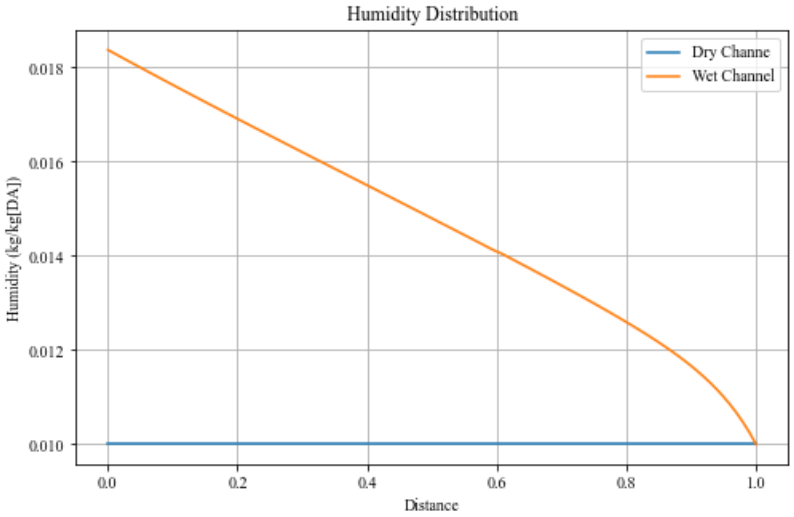


b

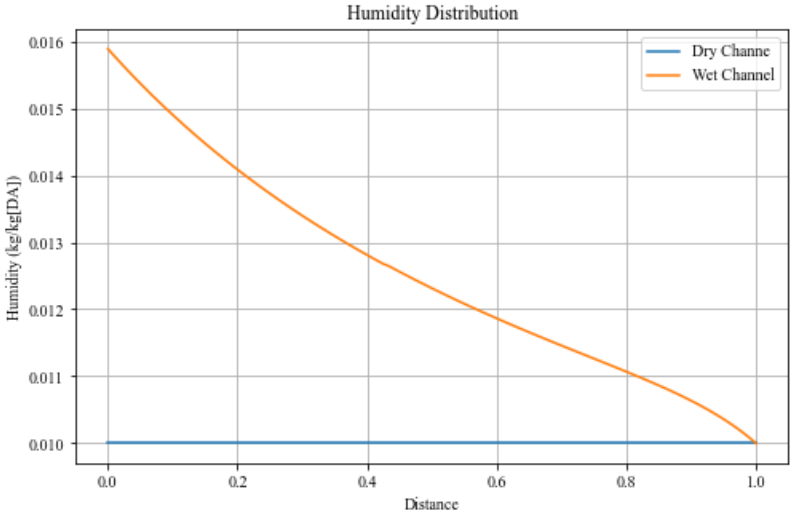


c

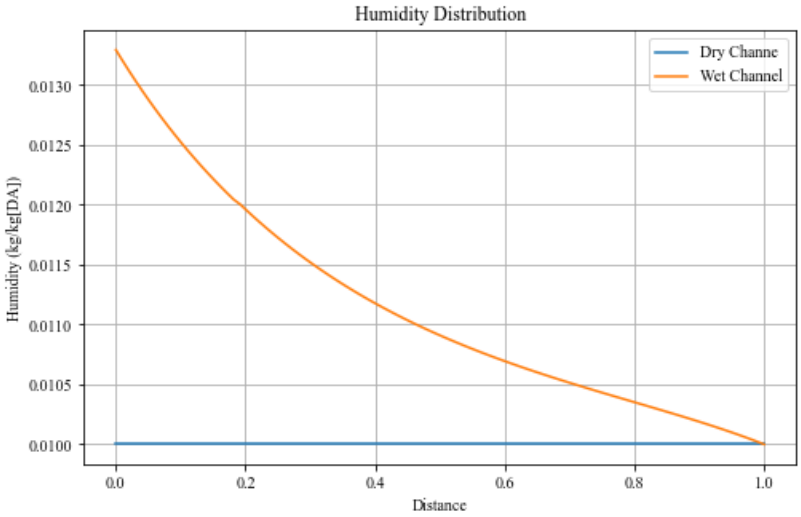


Fig.4.13 Humidity distribution of different working ratio: (a) 0.3; (b) 0.5; (c) 1.0.

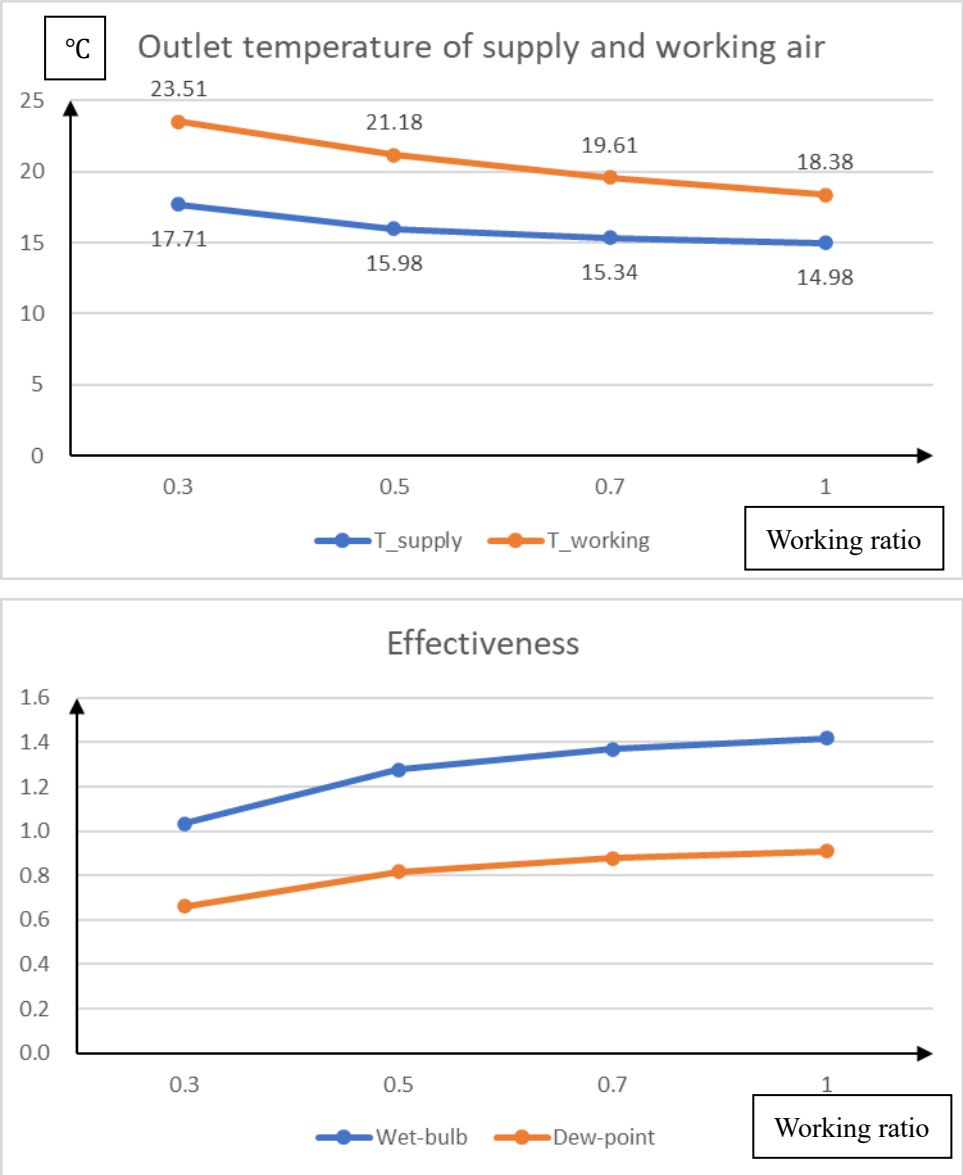


Fig.4.14 Comparison of output parameters at different working ratio.

The working ratio is another parameter that has an intense impact on the cooling performance of the system, strongly affecting the temperature and humidity distribution within the channel. With the increase of working ratio, the outlet temperature of working air and supply air decreases, and the wet bulb efficiency and dew point efficiency increase accordingly, which varies from 1.03 to 1.42 and 0.66 to 0.91. A larger working ratio means that more intake air enters the wet channel and becomes working air. The increased amount of working air in the wet channel requires more intense heat and mass transfer processes, which is reason why the temperature of supply air decrease. On the other hand, the increase in the amount of working air is greater than the increase in heat exchange in the channel, therefore the outlet temperature of the working air is also reduced.

### 4.2.5 Channel length

The channel length varies from 0.2m to 1.5m.

a

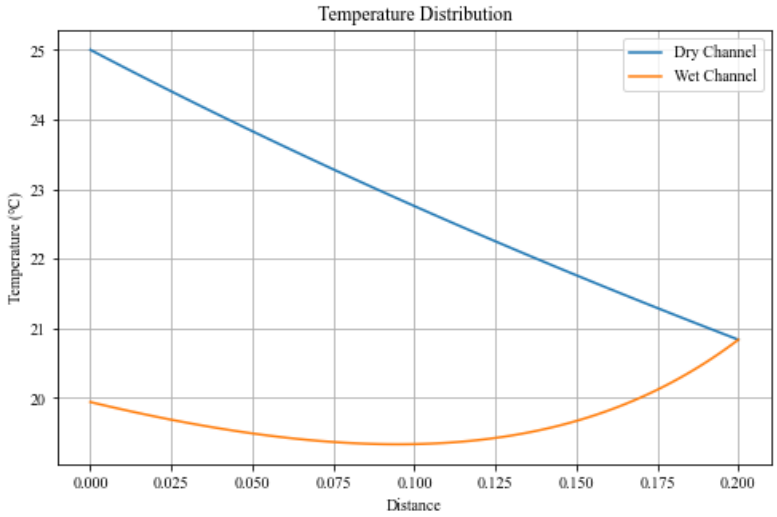


b

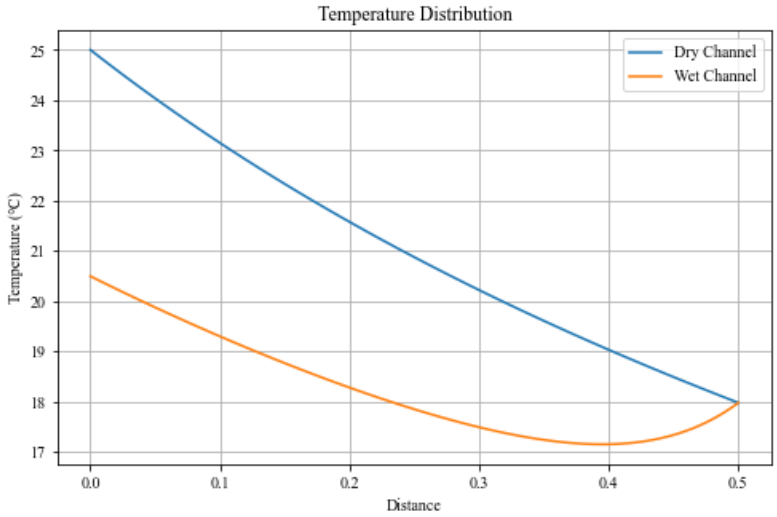


c

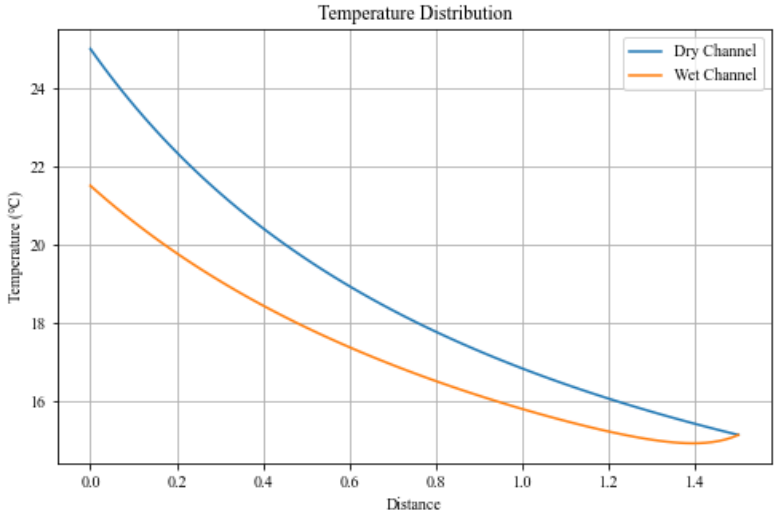


Fig.4.15 Temperature distribution of different channel length: (a) 0.2m; (b) 0.5m; (c) 1.5m.

a

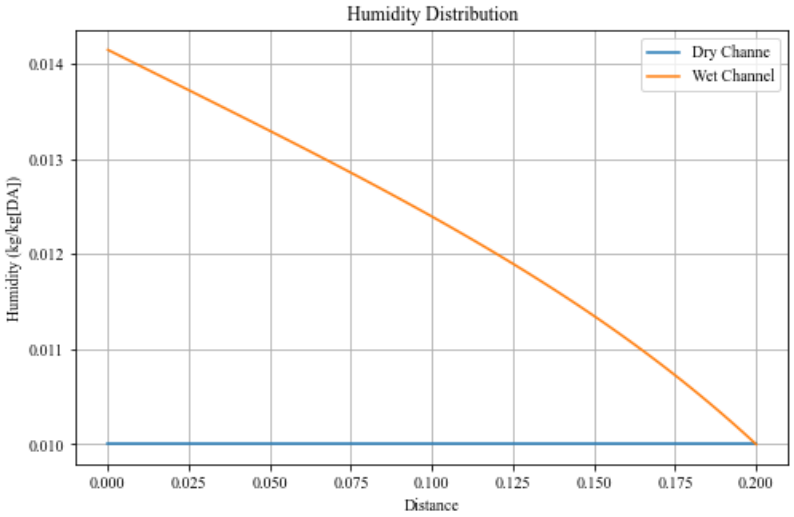


b

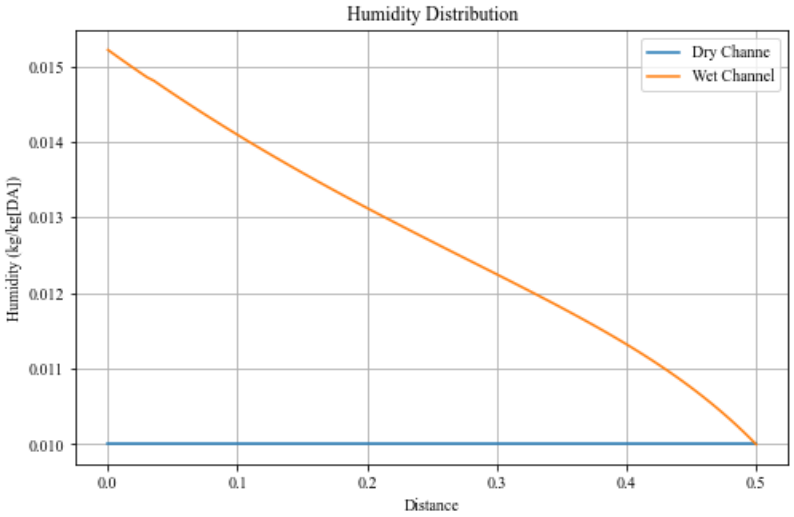


c

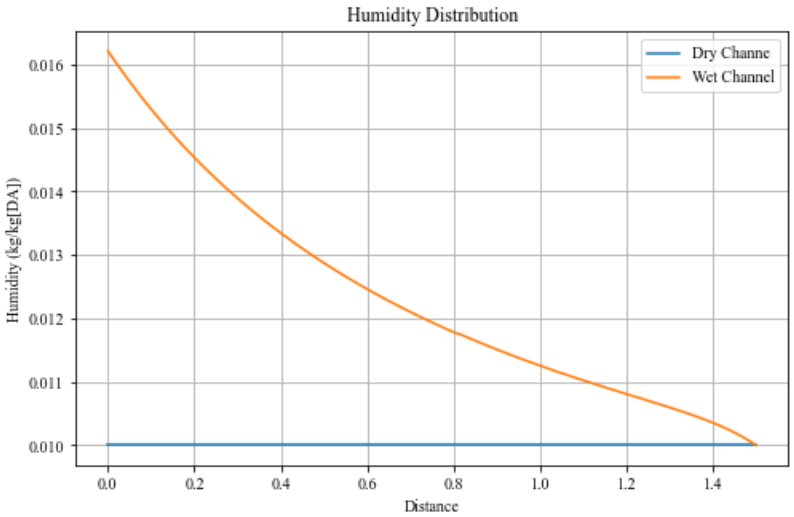


Fig.4.16 Humidity distribution of different channel length: (a) 0.2m; (b) 0.5m; (c) 1.5m.

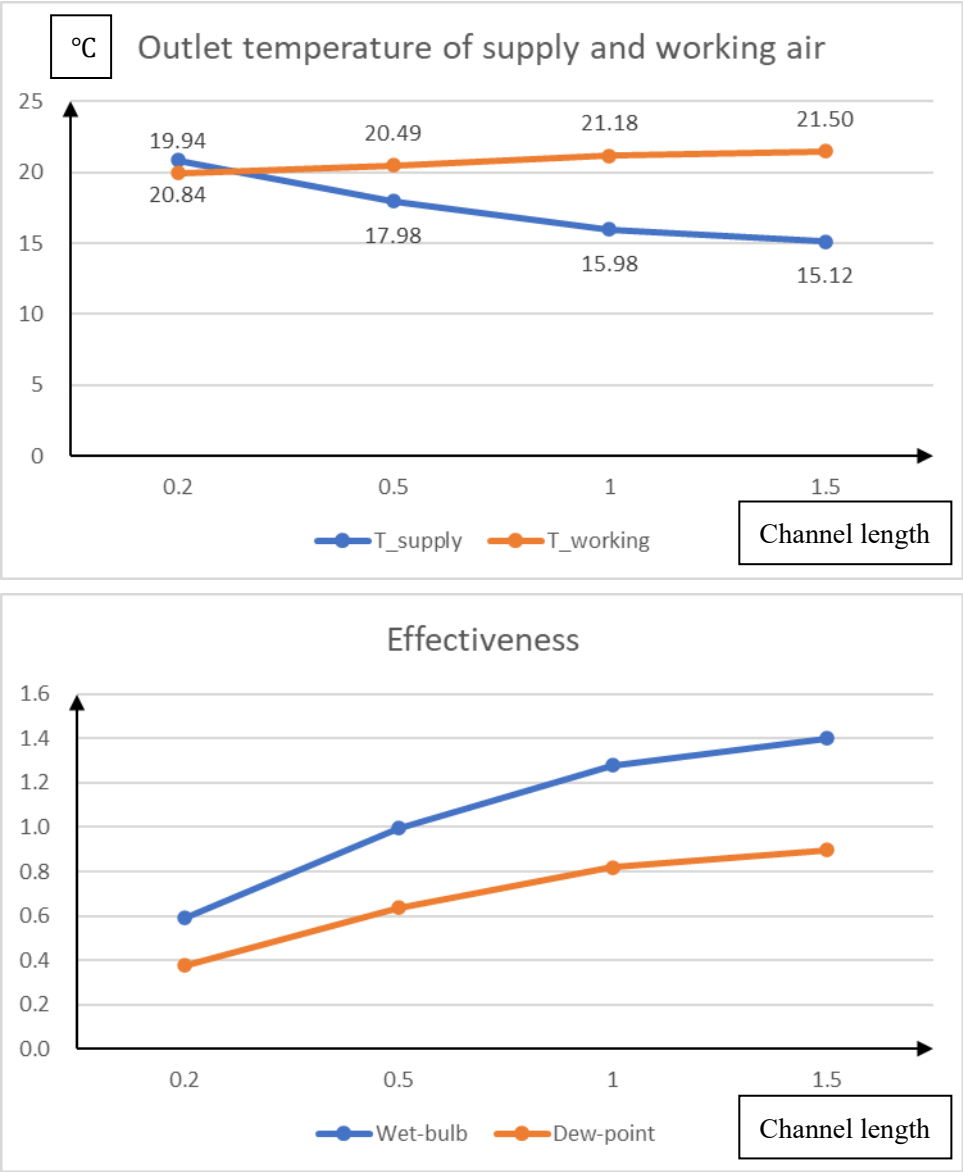


Fig.4.17 Comparison of output parameters at different channel length.

As can be seen from the above figure, the length of the channel also has a great influence on the performance of the system, because the length of the channel affects the area of heat and mass transfer and whether the working air can reach saturation in the channel. As the channel length increases, the supply air outlet temperature decreases, the working air outlet temperature increases, and the wet bulb efficiency and dew point efficiency also increase, which varies from 0.59 to 1.39 and 0.38 to 0.90. This is because longer channels mean more heat and mass transfer processes. As an example of extreme working conditions, when the channel length is 0.2m, after the temperature of the working air reaches the lowest point in the wet channel (same as the water film), the temperature only rises a little and then leaves the channel. At this time, the working air has not yet reached saturation, which is why the wet bulb efficiency is less than 1 and the outlet working air temperature is less than the outlet supply air temperature.

### 4.2.6 Channel height

The channel height varies from 2.5 mm to 8.5 mm.

a

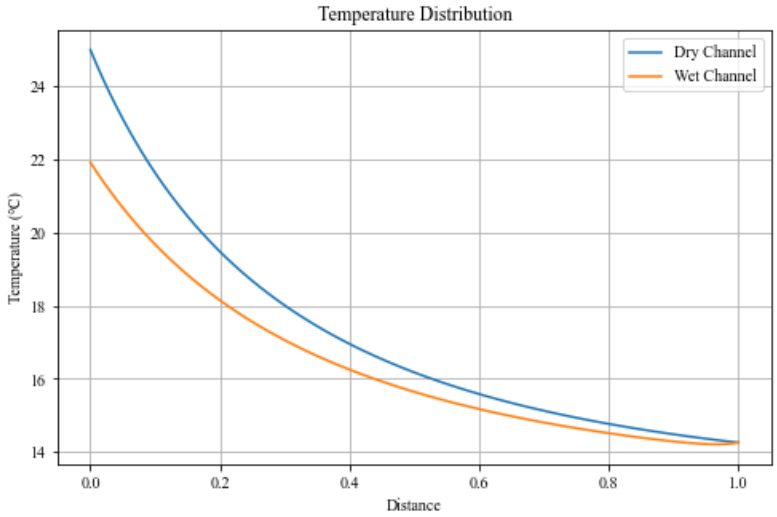


b

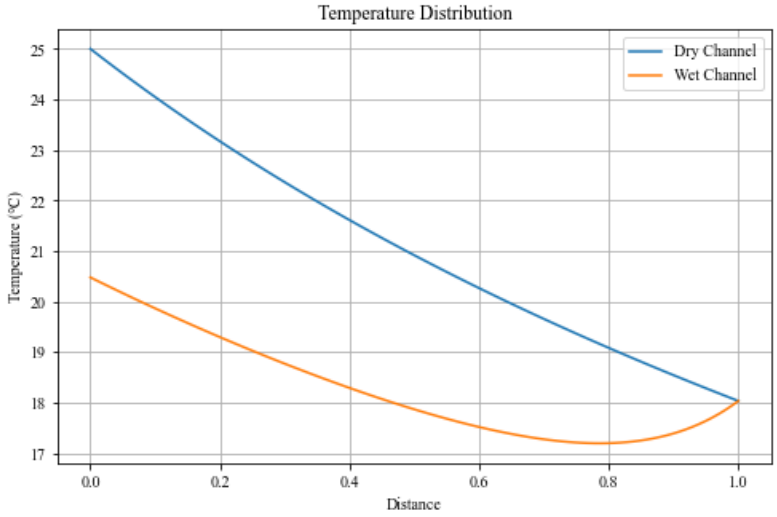


c

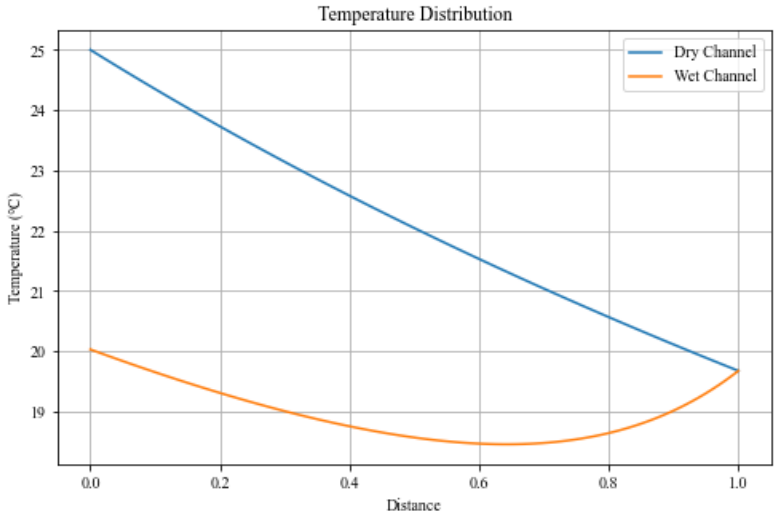


Fig.4.18 Temperature distribution of different channel height: (a) 0.0025m; (b) 0.0065m; (c) 0.0085m.

a

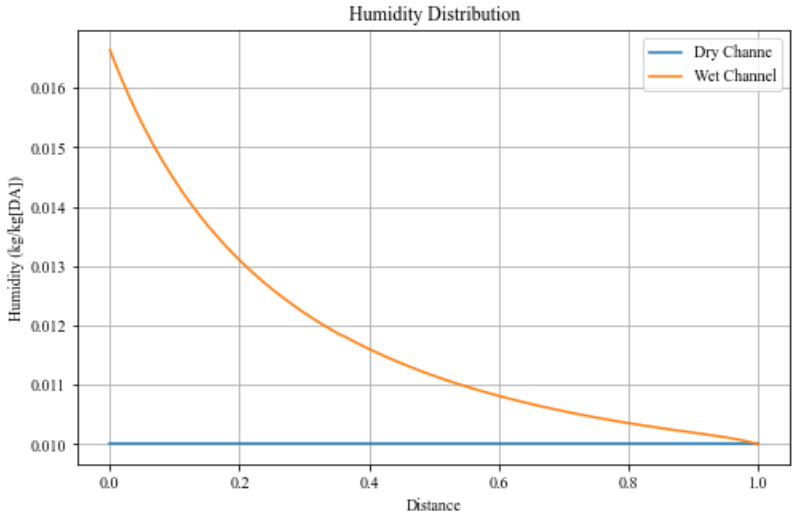


b

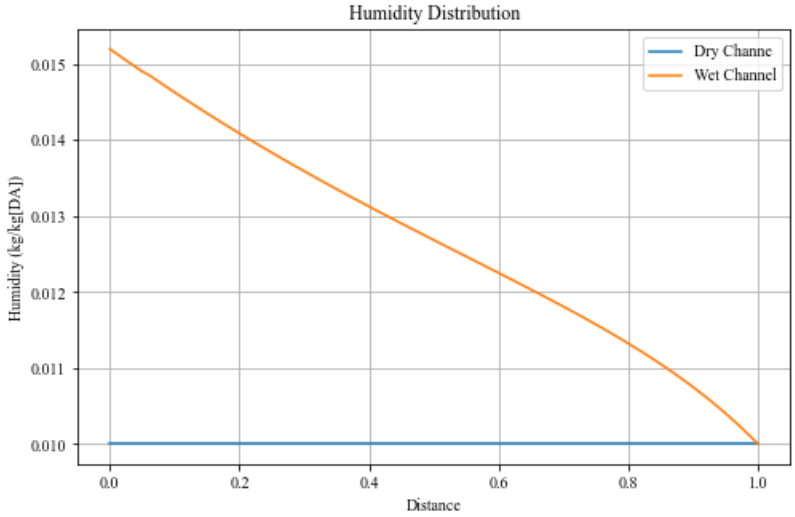


c

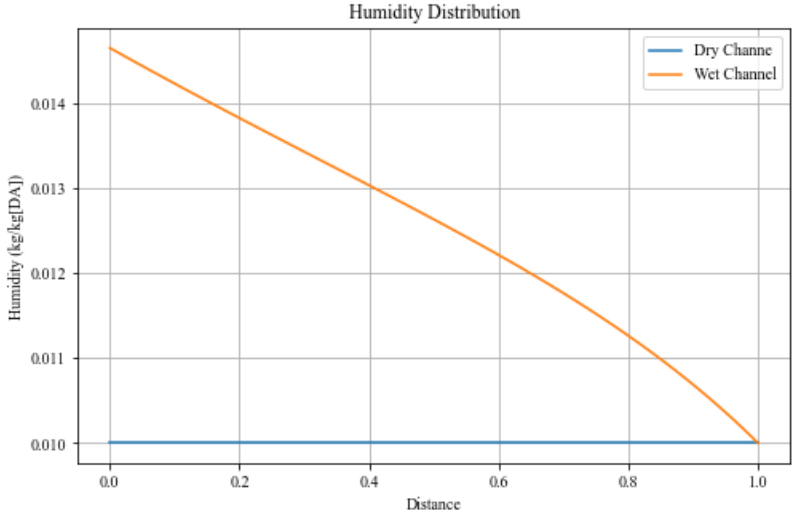


Fig.4.19 Humidity distribution of different channel height: (a) 0.0025m; (b) 0.0065m; (c) 0.0085m.

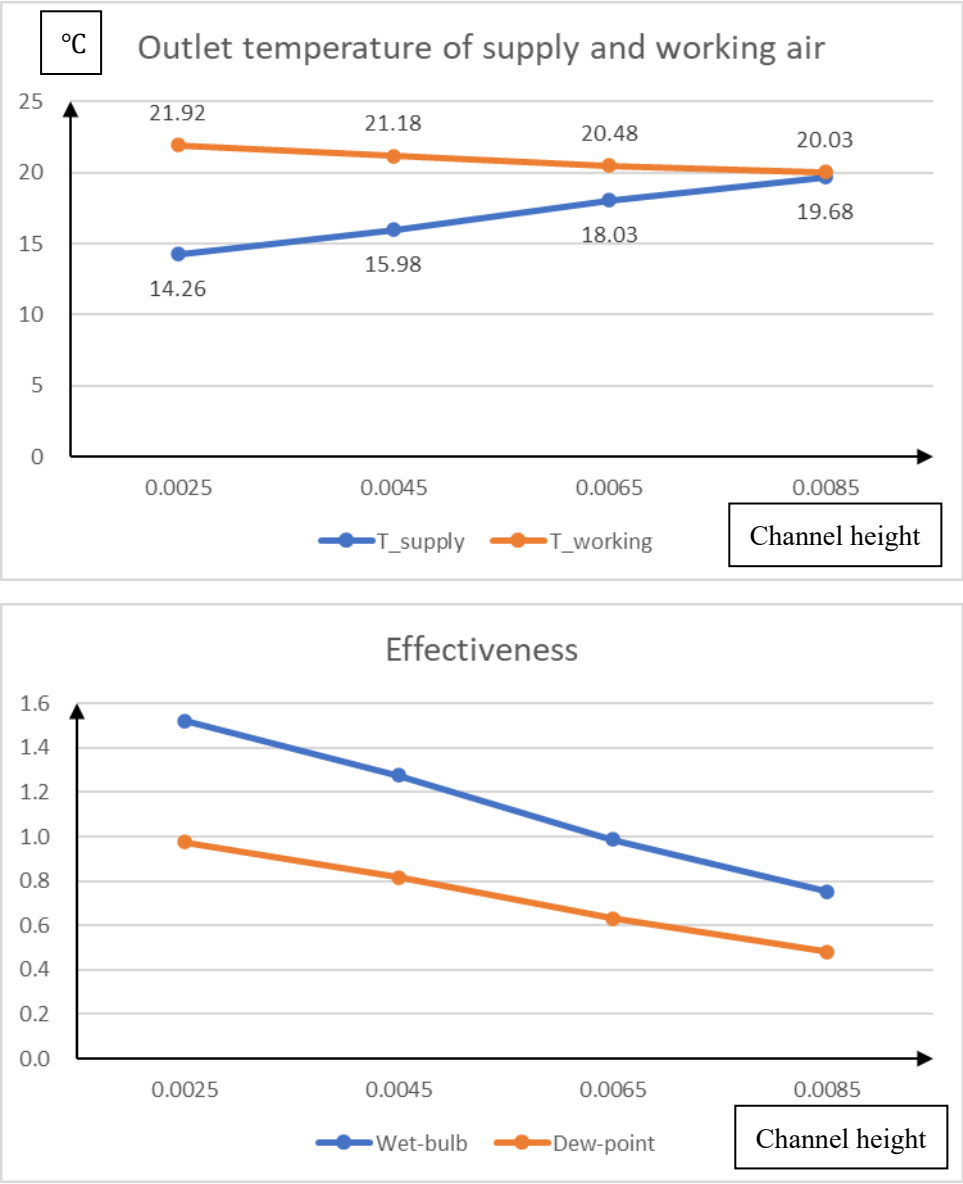


Fig.4.20 Comparison of output parameters at different channel height.

Another geometric parameter that has a significant impact on system performance is the height of the channel, as its value directly determines the hydraulic diameter of the system and further affect the value of heat and mass transfer coefficient. The outlet temperature of supply air is gradually reducing with the decreasing of the channel height. On the other hand, the wet bulb and dew point efficiencies decrease with increasing channel height, which varies from 1.52 to 0.75 and 0.98 to 0.48. Similarly, under extreme conditions (channel height equal to 8.5mm), the working air is not saturated.

## 4.3 Chapter summary

In this chapter, several parameters that may affect the performance of the system are analyzed using the simulation model validated in Chapter 3. The temperature and humidity distribution diagrams in the dry and wet channels under different variables are obtained, and the degree of influence on the system performance under different working conditions is also compared.

# Chapter 5 Summary

This paper focuses on the study and analysis of a single stage two-channel counter-flow m-cycle system. The m-cycle system is learned mainly through two aspects: simulation and experiment. On the one hand, through the existing knowledge of heat transfer and mass transfer, learn the heat and mass transfer process between wet and dry channels, channel walls, and water film, establish appropriate mathematical models, and complete the calculation of system equations through Python. After the basic simulation calculation is completed, various parameters affecting the performance are analyzed and calculated. On the other hand, an actual m-cycle experimental setup is established to learn the actual performance of the m-cycle system under non-ideal conditions and to use the results of the experimental setup to verify the accuracy of the simulation model.

In the chapter 1, the current situation of the environment, the general situation of evaporative cooling system, the basic concept and principle of m-cycle are introduced first. And scholars' research on m-cycle, including simulation and experiment are summarized. Finally, the purpose and objectives of this paper are introduced.

In the chapter 2, Using the principles and knowledge of heat transfer and mass transfer, the dry channel, wet channel, water film and channel plate of the 2-channel m-cycle system are analyzed, and the system equation is established. Under the steady state and specific conditions of m-cycle system operation, the system equations are simplified to ordinary differential equations, the Powell method is used to solve the equation system, and the solution of ordinary differential equations is calculated through Python. In this chapter, it focuses on how to establish a mathematical model and the solution steps of Powell's method.

In the chapter 3, the construction process of a simple 2-channel, counter-flow m-cycle system test bench is described in detail. The test bench consists of four main components: water supply system, air supply system, sensors and the main m-cycle unit. This chapter describes how to simulate the water layer in the wet channel in the experiment (using wick material and continuous water supply to the material), the air path of the wet and dry channel in the m-cycle, and what test points the system has. The environmental conditions in which the bench is located and how the parameters are changed. Through the data obtained from this prototype test bench and the simulation results, the following conclusions can be drawn:

1) The experiment tested the outlet temperature of supply air and working air under different conditions of inlet air temperature, inlet air humidity, inlet air velocity and working ratio, and compared these data with the simulation results. The results showed that there was an error between the two. The range is between 3% and 30%, and most data are within 15% error.

2) Considering the actual operating conditions, there are inevitable air leakage and pressure reduction in the channel. It can be considered that to a certain extent, the simulation model can correctly simulate the performance of the m-cycle system.

In the chapter 4, The results of the simulation model for a single working condition are shown and explained. By changing the inlet air parameters: temperature, humidity, velocity, working ratio, and system geometry parameters: the length and height of the channel, the influence of the change of parameters on the distribution of temperature and humidity in the channel and the wet bulb and dew point efficiency of the system are analyzed and studied. Based on the above simulation conditions, the following conclusions can be obtained:

1) The temperature of the supply air will decrease as the inlet air temperature and humidity decrease. However, the effect of inlet air parameters (temperature and humidity) on wet bulb efficiency is negligible. Dew point efficiency increases with higher inlet air temperature and humidity ratio in most of cases.

2) The effect of inlet air velocity and working ratio on the heat and mass transfer process of the system is significant due to the change of Reynolds and Nusselt number. By changing the velocity from 1 m/s to 3 m/s, the wet bulb effectiveness can be changed from 1.38 to 0.96, while dew point effectiveness is from 0.88 to 0.62. Similarly, in the working ratio case, the wet bulb effectiveness is from 1.03 to 1.42, while dew point is from 0.66 to 0.91.

3) The length and height of the channel also have a significant impact on the cooling process of the system, since these two parameters directly affect the hydraulic diameter and heat exchange area of the system. The temperature of the supply air decreases with increasing channel length and decreasing height. Likewise, wet bulb efficiency and dew point efficiency increase with increasing channel length and decreasing height. However, changing these two parameters brings some extreme conditions, that is, the outlet working air could not reach the saturation state, which resulted in extremely low wet bulb and dew point efficiency of the system. This means that the variation range of air parameters should be fully considered when designing the geometry of the m-cycle system.

Based on the above content, this thesis starts to study and analyze the 2-channel counter-current m-cycle system from both simulation and experiment, and analyzes the influence of these variables on the system performance by changing different parameters. It can be considered that the operation principle of the 2-channel m-cycle system is well demonstrated, and the influence of variable parameters on system performance is analyzed, which can provide ideas for improving system efficiency.

# Acknowledgement

First of all, I would like to express my sincere thanks to Professor Miyazaki Takahiko of Interdisciplinary Graduate School of Engineering Sciences (IGSES), Kyushu University. I would like to thank my professor for giving me the opportunity to study in Japan, for giving me a lot of help in various procedures and study studies in Japan, and for providing careful answers and suggestions for research topics and research progress. I would like to express my heartfelt thanks to the teachers for Prof. Miyazaki Takahiko meticulous care over the past two years.

I would like to express my sincere thanks to Kyaw Thu, Associate Professor of Interdisciplinary Graduate School of Engineering Sciences (IGSES), Kyushu University. As my tutor, he gave me professional and meticulous guidance in terms of mathematical models, computer language learning, course teaching, and various details of building experimental benches, which helped me to learn a lot of professional knowledge efficiently and quickly during my master's degree, enriched my resume, improved my level and increased my experience. Being a professor and being a friend has a profound impact on my life. I would like to express my sincere thanks to the Prof. Kyaw Thu.

I would like to express my sincere thanks to Frantisek Miksik, Assistant Professor at Interdisciplinary Graduate School of Engineering Sciences (IGSES), Kyushu University. With his rich experimental experience and professional knowledge, Prof. Miksik taught me the realization methods of various components during the construction of the experimental bench, and gave me many professional and efficient suggestions and guidance. I would like to express my sincere thanks to Prof. Frantisek Miksik.

I would like to express my sincere thanks to Takata Nobuo, the technician of Interdisciplinary Graduate School of Engineering Sciences (IGSES), Kyushu University. The safety education, the acquisition of experimental parts, and the technical expertise provided during the study helped me a lot and benefited a lot. I would like to express my sincere thanks to the Takata technicians.

I would like to express my sincere thanks to Yamato Yuri, the Secretary of Miyazaki Lab, Interdisciplinary Graduate School of Engineering Sciences (IGSES), Kyushu University. The processing of various documents during the study period, the reimbursement for the purchase of experimental objects, and various notices related to the study abroad program have provided great help for my study abroad life. I would like to express my sincere thanks to Secretary Yamato.

I would like to express my sincere thanks to all the members of the Miyazaki Lab, Interdisciplinary Graduate School of Engineering Sciences (IGSES), Kyushu

University, for bringing guidance and experience to my study and bringing warmth and excitement to my daily life. I would like to express my sincere thanks to them.

Finally, I would like to express my sincere thanks to my parents and family members who have always supported my study abroad life.

# References


[1] International Energy Agency (IEA), "'The Future of Cooling Opportunities for energy- efficient air conditioning'International Energy Agency Website: www.iea.org, 2018," 2018, [Online]. Available: www.iea.org.

[2] Q. Chen, K. Yang, M. Wang, N. Pan, and Z. Y. Guo, "A new approach to analysis and optimization of evaporative cooling system I: Theory," *Energy*, vol. 35, no. 6, pp. 2448–2454, 2010, doi: 10.1016/j.energy.2010.02.037.

[3] Q. Chen, N. Pan, and Z. Y. Guo, "A new approach to analysis and optimization of evaporative cooling system II: Applications," *Energy*, vol. 36, no. 5, pp. 2890–2898, 2011, doi: 10.1016/j.energy.2011.02.031.

[4] V. Maisotsenko, "Method and Plate Apparatus for Dew Point Evaporative Cooler," *Control Eng.*, vol. 53, no. 9, pp. 12–15, 2003.

[5] D. Tertipis and E. Rogdakis, "Maisotsenko cycle: technology overview and energy-saving potential in cooling systems," *Energy Emiss. Control Technol.*, p. 15, 2015, doi: 10.2147/eect.s62995.

[6] L. Elberling, "Laboratory Evaluation of the Coolerado Cooler Indirect Evaporative Cooling Unit," *Pacific Gas Electr. Co.*, no. 1, 2006, [Online]. Available: http://scholar.google.com/scholar?hl=en&btnG=Search&q=intitle:Laboratory+Evaluation+of+the+Coolerado+Cooler+Indirect+Evaporative+Cooling+Unit#0.

[7] X. Zhao, J. M. Li, and S. B. Riffat, "Numerical study of a novel counter-flow heat and mass exchanger for dew point evaporative cooling," *Appl. Therm. Eng.*, vol. 28, no. 14–15, pp. 1942–1951, 2008, doi: 10.1016/j.applthermaleng.2007.12.006.

[8] G. Heidarinejad and S. Moshari, "Novel modeling of an indirect evaporative cooling system with cross-flow configuration," *Energy Build.*, vol. 92, pp. 351–362, 2015, doi: 10.1016/j.enbuild.2015.01.034.

[9] S. Anisimov and D. Pandelidis, "Numerical study of the Maisotsenko cycle heat and mass exchanger," *Int. J. Heat Mass Transf.*, vol. 75, pp. 75–96, 2014, doi: 10.1016/j.ijheatmasstransfer.2014.03.050.

[10] S. Anisimov, D. Pandelidis, A. Jedlikowski, and V. Polushkin, "Performance investigation of a M (Maisotsenko)-cycle cross-flow heat exchanger used for indirect evaporative cooling," *Energy*, vol. 76, pp. 593–606, 2014, doi: 10.1016/j.energy.2014.08.055.

[11] S. Anisimov, D. Pandelidis, and J. Danielewicz, "Numerical analysis of selected evaporative exchangers with the Maisotsenko cycle," *Energy Convers. Manag.*, vol. 88, pp. 426–441, 2014, doi: 10.1016/j.enconman.2014.08.055.

[12] D. Pandelidis, S. Anisimov, and W. M. Worek, "Comparison study of the counter-flow regenerative evaporative heat exchangers with numerical methods," *Appl. Therm. Eng.*, vol. 84, pp. 211–224, 2015, doi: 10.1016/j.applthermaleng.2015.03.058.

[13] A. Hasan, “Going below the wet-bulb temperature by indirect evaporative cooling: Analysis using a modified ε-NTU method,” *Appl. Energy*, vol. 89, no. 1, pp. 237–245, 2012, doi: 10.1016/j.apenergy.2011.07.005.
[14] A. Hasan, “Indirect evaporative cooling of air to a sub-wet bulb temperature,” *Appl. Therm. Eng.*, vol. 30, no. 16, pp. 2460–2468, 2010, doi: 10.1016/j.applthermaleng.2010.06.017.
[15] J. Lin, K. Thu, T. D. Bui, R. Z. Wang, K. C. Ng, and K. J. Chua, “Study on dew point evaporative cooling system with counter-flow configuration,” *Energy Convers. Manag.*, vol. 109, pp. 153–165, 2016, doi: 10.1016/j.enconman.2015.11.059.
[16] C. Zhan, X. Zhao, S. Smith, and S. B. Riffat, “Numerical study of a M-cycle cross-flow heat exchanger for indirect evaporative cooling,” *Build. Environ.*, vol. 46, no. 3, pp. 657–668, 2011, doi: 10.1016/j.buildenv.2010.09.011.
[17] B. Riangvilaikul and S. Kumar, “An experimental study of a novel dew point evaporative cooling system,” *Energy Build.*, vol. 42, no. 5, pp. 637–644, 2010, doi: 10.1016/j.enbuild.2009.10.034.
[18] Z. Duan, “Investigation of a novel dew point indirect evaporative air conditioning system for buildings,” *Phd Diss.*, no. September, 2011, [Online]. Available: http://etheses.nottingham.ac.uk/12200/.
[19] C. Zhan, Z. Duan, X. Zhao, S. Smith, H. Jin, and S. Riffat, “Comparative study of the performance of the M-cycle counter-flow and cross-flow heat exchangers for indirect evaporative cooling - Paving the path toward sustainable cooling of buildings,” *Energy*, vol. 36, no. 12, pp. 6790–6805, 2011, doi: 10.1016/j.energy.2011.10.019.
[20] M. Jradi and S. Riffat, “Experimental and numerical investigation of a dew-point cooling system for thermal comfort in buildings,” *Appl. Energy*, vol. 132, pp. 524–535, 2014, doi: 10.1016/j.apenergy.2014.07.040.
[21] J. Lee and D. Y. Lee, “Experimental study of a counter flow regenerative evaporative cooler with finned channels,” *Int. J. Heat Mass Transf.*, vol. 65, pp. 173–179, 2013, doi: 10.1016/j.ijheatmasstransfer.2013.05.069.
[22] F. Bruno, “On-site experimental testing of a novel dew point evaporative cooler,” *Energy Build.*, vol. 43, no. 12, pp. 3475–3483, 2011, doi: 10.1016/j.enbuild.2011.09.013.
[23] A. Pakari and S. Ghani, “Comparison of 1D and 3D heat and mass transfer models of a counter flow dew point evaporative cooling system: Numerical and experimental study,” *Int. J. Refrig.*, vol. 99, pp. 114–125, 2019, doi: 10.1016/j.ijrefrig.2019.01.013.
[24] Z. Duan *et al.*, “Indirect evaporative cooling: Past, present and future potentials,” *Renew. Sustain. Energy Rev.*, vol. 16, no. 9, pp. 6823–6850, 2012, doi: 10.1016/j.rser.2012.07.007.
[25] T. Miyazaki and V. S. Maisotsenko, “Potential of an Ambient Air for Energy Saving Technologies through the Maisotsenko Cycle Evaporative Cooling,” 2018.
[26] K. Matsui, K. Thu, and T. Miyazaki, “A hybrid power cycle using an inverted

Brayton cycle with an indirect evaporative device for waste-heat recovery," *Appl. Therm. Eng.*, vol. 170, no. December 2019, p. 115029, 2020, doi: 10.1016/j.applthermaleng.2020.115029.

[27] J. Lin *et al.*, "Unsteady-state analysis of a counter-flow dew point evaporative cooling system," *Energy*, vol. 113, pp. 172–185, 2016, doi: 10.1016/j.energy.2016.07.036.

[28] Bergman, Theodore L., et al. *Fundamentals of heat and mass transfer*. John Wiley & Sons, 2011.